POLITECNICO DI TORINO
Repository ISTITUZIONALE

Robust adaptive control for aggressive quadrotor maneuvers via SO(3) and backstepping techniques

Publisher copyright

(Article begins on next page)
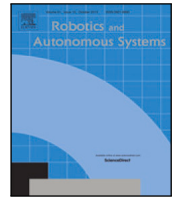
09 March 2025

Robust adaptive control for aggressive quadrotor maneuvers via SO(3) and backstepping techniques

Weibin Gu [a,c], Stefano Primatesta [b], Alessandro Rizzo [a,*]

[a] *Department of Electronics and Telecommunications, Politecnico di Torino, Turin, 10129, Italy*
[b] *Department of Mechanical and Aerospace Engineering, Politecnico di Torino, Turin, 10129, Italy*
[c] *Institute for AI Industry Research (AIR), Tsinghua University, Beijing, 100084, PR China*

ARTICLE INFO

ABSTRACT

For decades, a number of nonlinear control methodologies such as backstepping control and model predictive control have been studied to guarantee the stability and performance of systems under control. Most of these designs were based on local coordinates like Euler angles or quaternions, coming with inherent limitations such as singularities and unwinding phenomena, thereby hindering practical applications where large angle rotational maneuvers are commanded. In this paper, we propose a novel adaptive geometric tracking controller based on the logarithmic map of SO(3), the special orthogonal group, for aggressive maneuvers of a quadrotor subject to uncertain mass and inertia matrix. By directly synthesizing control laws on SO(3), issues raised by local coordinates can be circumvented. Furthermore, we provide theoretical proofs establishing asymptotic tracking and the boundedness of all signals in the closed-loop system. We enhance robustness by applying projection operators to adaptive laws, addressing nonparametric uncertainties like sensor noise. Through simulation, our proposed controller outperforms prior geometric controllers in tracking aggressive trajectories, particularly excelling in the face of uncertainties.

1. Introduction

In recent years, quadrotors have garnered substantial attention and demonstrated significant utility in various aspects of our daily lives, spanning from entertainment, such as aerial photography, to meeting industrial demands such as delivery of goods and infrastructure inspection, just to list a few [1–4]. This is attributed by and large to their high mobility, vertical take-off and landing capability, as well as low maintenance cost. Nonetheless, the design of controllers for quadrotors toward trajectory tracking or attitude stabilization is non-trivial due to the inherent nonlinearities and strong coupling properties in quadrotor dynamics, let alone uncertainties and disturbances, which are ubiquitous in real-world flight operations [5]. The challenge escalates even more when the quadrotor is assigned to perform aggressive maneuvers, particularly for specific tasks such as aerial acrobatics or rapid changes in direction [6,7].

For decades, a number of nonlinear control methodologies have been studied to guarantee stability and performance of systems under control; see, e.g., Backstepping Control (BSC) [8], Sliding Mode Control (SMC) [9], Model Predictive Control (MPC) [10], and Disturbance-observer-based Control (DOBC) [11]. Most of these designs were based on *local coordinates* such as Euler angles and quaternions to describe

the rotational kinematics and dynamics of quadrotors. Despite merits, such as quaternions being the minimal representation without singular points [12], and Euler angles providing an intuitive representation for 3-D rotations, local coordinates come with inherent limitations that hinder practical applications, especially for aggressive maneuvers [13]. Specifically, the Gimbal lock (or singularity), arisen from Euler angles, results in the loss of one degree of freedom in 3-D orientation systems [14]; Unwinding phenomena related to quaternion representations can cause rotations through large angles before stabilizing at the desired attitude, even with a close initial state [15]. These issues are particularly undesirable in aerospace applications, as they may induce catastrophic instability.

Geometric control techniques have recently been proven to be effective in tackling these issues, especially in the execution of aggressive maneuvers; see, e.g., [16–22]. Instead of using local coordinates, geometric controllers are designed directly on the *special orthogonal group* SO(3), which is a nonlinear manifold on which the configuration space of attitude dynamics evolves. For example, one of the first applications of geometric control to quadrotors was [16], where a controller was proposed on the nonlinear configuration Lie group. As such, through the intrinsic characterization of the geometric properties

of nonlinear manifolds, singularities and ambiguities associated with local coordinates can be circumvented, thereby enabling the execution of large-angle rotational maneuvers.

While notable advancements have been made in geometric control for quadrotors, crucial gaps persist, particularly in addressing uncertainties and disturbances, as well as in selecting configuration error functions. Like other model-based control approaches, the effectiveness of the control law derived from SO(3) hinges on the precise knowledge of the system parameters. Additionally, the exploration of configuration error functions for control synthesis remains an open topic in geometric control, sometimes chosen without careful consideration. Although some studies draw on the results in [16] (see, e.g., [1,3,18,20,23]), it was observed that the chosen configuration error vector can lead to degraded performance with increasing initial attitude error, prompting a new error function proportional to the rotation angle for consistent tracking performance [17]. Another alternative for the configuration error function is the logarithmic map of SO(3) [24]. Thanks to the inherent ability to transform geodesics on SO(3) into straight lines in its Lie algebra $\mathfrak{so}(3)$, the logarithmic map establishes a proportional relationship between the magnitude of the attitude error vector and the rotation angle, with a higher proportionality constant than that used in [17], hence facilitating accelerated convergence rates for tracking errors [22,25]. However, existing studies in this direction focus only on the nominal case, neglecting uncertainties and disturbances, which could potentially compromise controller performance or even lead to instability in the worst condition.

In this work, we present a novel robust adaptive geometric controller for aggressive quadrotor maneuvers in the presence of parametric uncertainties, namely the quadrotor mass and inertia matrix. While there are existing works using the special Euclidean group SE(3) on spacecraft control [26,27] taking into account the coupling between the translational and rotational dynamics, a common practice in quadrotor control is to decompose the problem into two distinct subtasks: position tracking in $\mathbb{R}^3$ and attitude tracking in SO(3) [28]. As illustrated in Fig. 1, our proposed method utilizes BSC for thrust determination and the logarithmic map of SO(3) to represent the attitude error for torque determination. In contrast to the existing approaches in [21,22] that employ the logarithmic map for nominal conditions, we present a fully nonlinear control synthesis with the capability to address uncertainties, thereby extending its applicability beyond linearized and uncertainty-free scenarios. Two adaptive laws are derived through Lyapunov analysis aimed at dynamically compensating for uncertainties in the mass and inertia matrix. Along with the use of projection operators [29], we show asymptotically stable tracking and the boundedness of all signals in the closed-loop system even when there exist non-parametric uncertainties such as sensor noise [30]. The main contributions of this paper are summarized as follows:

(i) We developed a novel adaptive geometric controller, leveraging the logarithmic map of SO(3) and BSC, for executing aggressive maneuvers without requiring precise knowledge of the mass and inertia matrix of the quadrotor.

(ii) We proved almost globally asymptotically stable tracking and the boundedness of all signals in the closed-loop system through Lyapunov analysis in the presence of non-parametric uncertainties.

(iii) We showed through simulation that the proposed controller outperforms prior studies [16,17,22] in tracking aggressive trajectories, particularly excelling in the face of uncertainties.

The remainder of this paper is organized as follows. Section 2 reviews the existing research in the field of geometric control for quadrotors. Section 3 introduces the notations and preliminary concepts used in the design of our controller, followed by the problem statement of this study. As the main results of this paper, Sections 4 and 5 elaborate the control synthesis of our proposed adaptive geometric tracking control for position and attitude with stability guarantees,

respectively. Theoretical proofs on asymptotic stability and the boundedness of all signals in the closed-loop system are also given therein. Section 6 demonstrates simulation results within MATLAB/Simulink environment, showcasing superior performance in tracking aggressive trajectories compared to prior geometric controllers, especially in handling parametric uncertainties. Finally, the paper draws to a close in Section 7 where we outline some directions for our future research.

2. Prior studies

Research endeavors in the domain of geometric control pertaining to quadrotors can be broadly categorized into two classes: one focuses on addressing uncertainties and disturbances, whereas the other centers around the selection of configuration error functions. A comparative analysis of previous studies is summarized in Table 1.

The first line of research aims to extend the results in [16] by taking into account uncertainties and disturbances. For example, [18] adopted integral control terms to guarantee almost global asymptotic stability when there exist fixed disturbances in both translational and rotational dynamics; [19] proposed a robust adaptive tracking controller without the knowledge of the inertia matrix and guaranteed the boundedness of tracking errors in the presence of unstructured disturbances; [20] developed adaptive control laws that guarantees asymptotic convergence of tracking errors for modeling error and uncertainties in dynamical equations; and [31] proposed an adaptive law for the geometric controller to estimate the center of gravity of the quadrotor, which differs from the geometric center. Other applications of tiltrotor [32] and load transportation quadrotor [1,3,23] can also be considered to fall into this class of studies.

Another avenue of research contributes to exploring configuration error functions, an ongoing subject in geometric control. These functions continue to be extensively examined and, at times, selected without meticulous consideration [17]. For example, the configuration error functions chosen in [16] may result in diminished performance as the initial attitude error tends to grow. To counteract this issue, several alternatives have been proposed to ensure consistent tracking performance by building a proportional relationship to the rotation angle. [17] adopted a revised version of [16] for the stabilization of a quadrotor subject to unknown inertia matrix; [25] designed a quadratic cost function in the Lie algebra through its gradient for the control on Lie groups thanks to their symmetry structure such that faster error convergence can be achieved; [21] proposed a Proportional-Integral-Derivative (PID) controller directly on $\mathfrak{so}(3)$, the Lie algebra associated with SO(3), with rotation modeled using exponential coordinates to perform complex acrobatic maneuvers; [33] employed a homogeneous method to address the finite-time control problem of a quadrotor on a Lie group, utilizing exponential and logarithmic maps; [22] presented a geometric tracking controller based on the logarithmic map of SO(3), achieving faster convergence speed of tracking error; [34] studied the performance of several attitude error vectors for the control of a quadrotor subject to rotor failures; and [35] proposed a hybrid attitude controller which guarantees global exponential stability and overcomes the topological obstacles of global control on SO(3) [13]. Nonetheless, almost none of these studies incorporate robust or adaptive designs to handle uncertainties and disturbances. Recently, [36] introduced an estimator-based approach that uses the logarithmic map of SO(3) to address disturbances in the tracking of multiple quadrotors. However, their controller was not evaluated under aggressive maneuvers. Our work differentiates itself by explicitly handling parametric uncertainties through adaptive laws.

3. Preliminaries and problem statement

Henceforth, we use case-sensitive bold symbols to represent multidimensional variables, e.g., $\mathbf{a}$ stands for a vector, while $\mathbf{A}$ stands for a matrix. The n-dimensional Euclidean space is denoted by $\mathbb{R}^n$ with
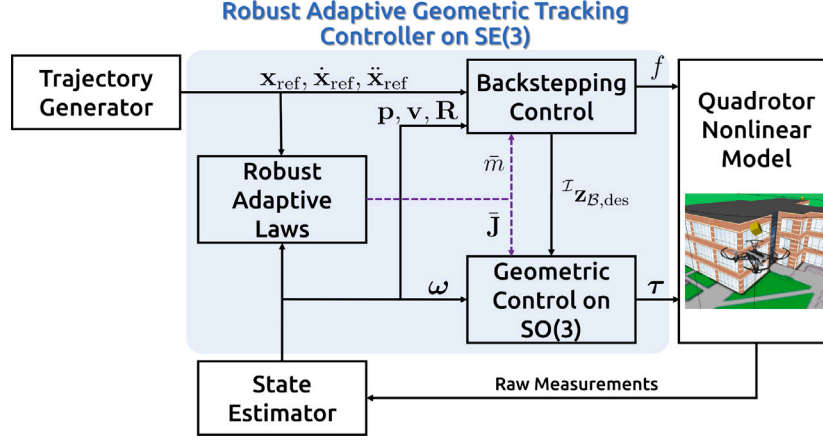
Fig. 1. Overall architecture of the proposed robust adaptive geometric tracking controller.

Table 1

A comparative analysis of selected literature on geometric control based on SO(3) with applications to quadrotors. We compared the error function for rotational configuration (2nd column), control methods for handling uncertainties (3rd column), and obtained results (4th column; *Num*: numerical, *Sim*: simulation, *Exp*: experimental). We kindly direct readers to Section 3 for detailed explanations of notations used.

Rotational error	Citation	Robustness and adaptability	Results
$\frac{1}{2}\operatorname{tr}(\mathbf{I}-\mathbf{R}_b^d)$	[16] (2010)	n/a	Num
	[18] (2013)	Integral control for handling constant disturbances	Num, Exp
	[20] (2014)	Adaptive laws for unmodeled dynamics	Num, Exp
	[23] (2018)	Control of quadrotor load transporting via rigid cables	Num
	[1] (2019)	Control of a quadrotor-pulley-load system	Num
	[3] (2021)	Control of quadrotor load transporting via elastic cables	Num
$2-\sqrt{1+\operatorname{tr}(\mathbf{R}_b^d)}$	[17] (2010)	Stabilization under an unknown inertia matrix	Num
$\frac{1}{2}\operatorname{tr}[\mathbf{G}(\mathbf{I}-\mathbf{R}_b^d)],\ \mathbf{G}>0$	[19] (2013)	A robust adaptive law for inertia matrix and bounded disturbances	Exp
	[31] (2020)	A robust adaptive law for center of gravity	Num
$\frac{1}{2}\operatorname{tr}[\mathbf{K}(\mathbf{I}-\mathbf{R}\mathbf{R}_d^\top)],\ \mathbf{K}>0$	[32] (2017)	Control of a tiltrotor	Num
$\|\log(\mathbf{R}_b^d)^\vee\|$	[21] (2015)	n/a	Exp
	[33] (2017)	n/a	Sim
	[22] (2021)	n/a	Sim, Exp
	[25] (2022)	n/a	Num
	[36] (2023)	A disturbance observer for handling time-varying disturbances	Sim
Hybrid error	[35] (2016)	n/a	Sim, Exp

the Euclidean norm $\|\cdot\|$. The transpose operator is denoted by $(\cdot)^\top$. The trace, determinant, and eigenvalues of a matrix are denoted by $\operatorname{tr}(\mathbf{A})$, $\det(\mathbf{A})$, and $\lambda(\mathbf{A})$, respectively. The Frobenius norm of a matrix is denoted by $\|\mathbf{A}\|_F = \sqrt{\operatorname{tr}(\mathbf{A}\mathbf{A}^\top)}$. The positive and semi-positive definiteness of a matrix is denoted by $\mathbf{A}>0$ and $\mathbf{A}\succeq 0$, respectively. The symbol $\mathbf{e}_3$ denotes a vector in the unit 2-sphere $\mathbb{S}^2 = \{\mathbf{a} \in \mathbb{R}^3 : \|\mathbf{a}\| = 1\}$ and $\mathbf{I}_n$ denotes $n \times n$ identity matrix. The hat operator is denoted by $(\cdot)^\wedge : \mathbb{R}^3 \rightarrow \mathfrak{so}(3)$ and inversely, the vee operator is denoted by $(\cdot)^\vee : \mathfrak{so}(3) \rightarrow \mathbb{R}^3$, where $\mathfrak{so}(3)$ represents the Lie algebra associated with a special orthogonal group $\mathrm{SO}(3) = \{\mathbf{R} \in \mathbb{R}^{3\times3} : \mathbf{R}^\top\mathbf{R} = \mathbf{I}_3, \det(\mathbf{R}) = 1\}$. The symbol $\mathcal{L}_\infty$ denotes the space of bounded functions and C^k ($k = 0, 1, 2, \ldots$) denotes the differentiability class of a function if its derivatives up to kth order exist and are continuous. To avoid confusion, the estimated variables are denoted by $(\bar{\cdot})$ instead of the conventional $(\hat{\cdot})$, and the error variables are denoted by $(\tilde{\cdot})$.

3.1. Quadrotor kinodynamic model

The continuous-time kinodynamic model of a quadrotor can be written in terms of differential equations as

$$^I\dot{\mathbf{p}} = {}^I\mathbf{v}, \tag{1}$$

$$^I\dot{\mathbf{v}} = g\mathbf{e}_3 - \frac{1}{m}f\mathbf{R}\mathbf{e}_3 + {}^I\mathbf{f}_{\text{ext}}, \tag{2}$$

$$\dot{\mathbf{R}} = \mathbf{R}\,{}^B\boldsymbol{\omega}^\wedge, \tag{3}$$

$$\mathbf{J}\,{}^B\dot{\boldsymbol{\omega}} = -{}^B\boldsymbol{\omega}^\wedge\mathbf{J}\,{}^B\boldsymbol{\omega} + {}^B\boldsymbol{\tau} + {}^B\boldsymbol{\tau}_{\text{ext}}, \tag{4}$$

where left superscripts $\{\mathcal{I}\}$ and $\{\mathcal{B}\}$ indicate inertial and body-fixed reference frame, respectively, for state variables following North-East-Down (NED) and Front-Right-Down (FRD) conventions. ${}^I\mathbf{p}, {}^I\mathbf{v} \in \mathbb{R}^3$ denote the position and linear velocity, ${}^B\boldsymbol{\omega} = [p, q, r]^\top \in \mathbb{R}^3$ denotes the body-fixed angular rate, $\mathbf{R} \in \mathrm{SO}(3)$ denotes the rotation matrix from $\{\mathcal{B}\}$ to $\{\mathcal{I}\}$ constructed by Euler angles ϕ, θ, ψ (i.e., roll, pitch, yaw) following the "3-2-1" convention, $f \in \mathbb{R}_{>0}, {}^B\boldsymbol{\tau} \in \mathbb{R}^3$ denote the thrust and torques produced by the four rotors (i.e., control inputs), ${}^I\mathbf{f}_{\text{ext}} \in \mathbb{R}^3, {}^B\boldsymbol{\tau}_{\text{ext}} \in \mathbb{R}^3$ denote the external forces and torques such as aerodynamic drag, $m \in \mathbb{R}, \mathbf{J} \in \mathbb{R}^{3\times3}$ denote the quadrotor mass and inertia matrix, and $g \in \mathbb{R}$ denotes the gravity constant. Note that the hat operator on $\boldsymbol{\omega}$ in (3) is equivalent to the skew-symmetric operator, which is the Lie algebra of SO(3),

$$\boldsymbol{\omega}^\wedge = \begin{bmatrix} 0 & -r & q \\ r & 0 & -p \\ -q & p & 0 \end{bmatrix} \in \mathfrak{so}(3), \tag{5}$$

and the rotation kinematics can also be expressed in form of other 3-D rotation representation such as Euler angles and quaternions at the cost of singularities and unwinding phenomenon as discussed in Section 1. In the sequel, we omit the left superscripts that indicate reference frames for brevity unless needed to clarify ambiguities.

Remark 1. It is worth noting that the modeling of forces and torques has been simplified by omitting the motor model, which can be typically represented as follows:

$$f_i = k_f n_i^2 \tag{6}$$

$$\tau_i = k_\tau n_i^2 \tag{7}$$

$$\dot{n}_i = k_m(n_i^{cmd} - n_i) \tag{8}$$

for $i = 1, 2, 3, 4$, where f_i, τ_i denote the force and torque generated by each rotor, n_i, n_i^{cmd} denote the executed and commanded angular speeds of each rotor in revolutions per minute, and k_f, k_τ, k_m denote the motor characteristic constants normally obtained through experimentation. These expressions have been omitted in (2) and (4), as the control inputs are directly formulated as forces and torques. Nonetheless, as will be shown in Section 6, we verify the performance of the controller with motor dynamics incorporated into the simulation, despite these dynamics not being explicitly modeled during the controller design phase. Moreover, given the scope of this study on parametric uncertainties in aggressive quadrotor maneuvers, the explicit handling of external forces and torques is beyond the scope of the current work and is left for future work.

3.2. Exponential and logarithmic map

The exponential map relates a matrix Lie group to its associated Lie algebra. For rotations, it can be computed through Rodrigues' rotation formula [37] as

$$\mathbf{R} = \exp(\boldsymbol{\phi}^\wedge) = \mathbf{I}_3 + \sin(\phi)\mathbf{a}^\wedge + (1 - \cos(\phi))\mathbf{a}^\wedge\mathbf{a}^\wedge, \tag{9}$$

where $\boldsymbol{\phi} = \phi\mathbf{a}$, $\mathbf{a} \in \mathbb{S}^2$ is the rotation axis, and $\phi \in \mathbb{R}$ is the rotation angle.[1]

The inverse of the exponential map is called logarithmic map [24] denoted as

$$\boldsymbol{\phi} = \log(\mathbf{R})^\vee, \tag{10}$$

which can be computed from

$$\phi = \arccos\left(\frac{\text{tr}(\mathbf{R}) - 1}{2}\right), \tag{11}$$

$$\boldsymbol{\phi} = \phi\mathbf{a} = \frac{\phi}{2\sin(\phi)}(\mathbf{R} - \mathbf{R}^\top)^\vee. \tag{12}$$

Remark 2. The exponential map from $\mathfrak{so}(3)$ to $SO(3)$ is surjective only, which means that there exist multiple candidates of $\mathfrak{so}(3)$ that produce the same element of $SO(3)$. This can be revealed by the fact that $\mathbf{R} = \exp((\phi + 2\pi n)\mathbf{a}^\wedge)$, with n being an arbitrary integer and the ambiguity in the sign of ϕ due to the even function $\cos(\phi)$. However, we can confine the map so that it is bijective by: (i) limiting $|\phi| < \pi$, and (ii) determining the correct sign of ϕ by verifying if the rotation matrix generated by such ϕ using (9) is correct; if not, reversing the sign of ϕ and recalculating the rotation axis. □

Finally, the left Jacobian of $SO(3)$ [24] is defined as

$$\mathbf{J}_l(\boldsymbol{\phi}) = \int_0^1 \exp(\boldsymbol{\phi}^\wedge)^\alpha d\alpha \tag{13}$$

$$= \frac{\sin(\phi)}{\phi}\mathbf{I}_3 + \left(1 - \frac{\sin(\phi)}{\phi}\right)\mathbf{a}\mathbf{a}^\top + \frac{1 - \cos(\phi)}{\phi}\mathbf{a}^\wedge, \tag{14}$$

and its inverse is given by

$$\mathbf{J}_l(\boldsymbol{\phi})^{-1} = \frac{\phi}{2}\cot\left(\frac{\phi}{2}\right)\mathbf{I}_3 + \left(1 - \frac{\phi}{2}\cot\left(\frac{\phi}{2}\right)\right)\mathbf{a}\mathbf{a}^\top - \frac{\phi}{2}\mathbf{a}^\wedge. \tag{15}$$

Remark 3. There exist singularities associated with $\mathbf{J}_l$ using the above equations due to the appearance of $\cot(\phi/2)$ at $\phi = 2\pi n$ with n being an arbitrary integer. To address this, we can use the approximation $\mathbf{J}_l(\boldsymbol{\phi}) \approx \mathbf{I}_3 + \frac{1}{2}\boldsymbol{\phi}^\wedge$ and $\mathbf{J}_l(\boldsymbol{\phi})^{-1} \approx \mathbf{I}_3 - \frac{1}{2}\boldsymbol{\phi}^\wedge$ [24]. □

3.3. Problem statement

Our control objective is to achieve asymptotically stable tracking for a quadrotor of a given, possibly aggressive reference trajectory $\mathbf{x}_{\text{ref}}(t)$ in the presence of an uncertain mass and inertia matrix while ensuring that all signals in the closed-loop system remain bounded.

To this end, we present a robust adaptive geometric tracking controller as illustrated in Fig. 1, which consists of: (i) a backstepping controller for thrust determination and providing attitude reference (in terms of body z-axis) to the inner-loop attitude controller, (ii) a geometric controller based on the logarithmic map of $SO(3)$ to generate commanded torques for attitude tracking, and (iii) two adaptive laws for handling uncertainties in mass and inertia matrix, robustified by projection operators. Throughout the control synthesis in Sections 4 and 5, we make the following assumptions and drop the time-dependent notation for simplicity.

Assumption 1. The reference trajectory is given in the form $\mathbf{x}_{\text{ref}}(t) = [\mathbf{p}_{\text{ref}}^\top(t) \ \psi_{\text{ref}}(t)]^\top \in \mathbb{R}^4$ using the differential flatness property of the quadrotors [38], which satisfies $\mathbf{x}_{\text{ref}}(t) \in C^3$, i.e., the derivatives up to $\mathbf{x}_{\text{ref}}^{(3)}(t)$ exist and are continuous.

Assumption 2. The derivatives up to the 3rd order of the reference trajectory are bounded, i.e., $\mathbf{x}_{\text{ref}}^{(k)}(t) \in \mathcal{L}_\infty$ ($k = 0, 1, 2, 3$).

Assumption 3. The quadrotor mass m and inertia matrix $\mathbf{J}$ are uncertain but slowly time-varying,[2] with their variations bounded, i.e., $\dot{m}, \dot{\mathbf{J}} \in \mathcal{L}_\infty$.

4. Thrust determination for position tracking

In this section, we present the primary results for achieving globally asymptotically stable tracking of position reference in the presence of uncertain mass through a backstepping formulation. To ensure the robustness of the adaptive law under nonparametric uncertainties such as sensor noise, a projection operator is applied to guarantee the boundedness of estimated parameters and avoid sudden instability.

Theorem 1 (*Adaptive Tracking Control for Translational Dynamics*)**.** *Consider the translational dynamics given by* (1), (2), *and for a given tracking command* $\mathbf{p}_{ref} \in C^3$, *we define the desired control input* (16) *and an adaptive law for mass estimation* (17) *as*

$$\mathbf{f} = \bar{m}(-\mathbf{K}_v\tilde{\mathbf{v}} - \tilde{\mathbf{p}} - g\mathbf{e}_3 + \dot{\mathbf{v}}_r), \tag{16}$$

$$\dot{\bar{m}} = \gamma_m\tilde{\mathbf{v}}^\top(\mathbf{K}_v\tilde{\mathbf{v}} + \tilde{\mathbf{p}} + g\mathbf{e}_3 - \dot{\mathbf{v}}_r), \tag{17}$$

$$\mathbf{v}_r = \dot{\mathbf{p}}_{ref} - \mathbf{K}_p\tilde{\mathbf{p}}, \tag{18}$$

where $\gamma_m \in \mathbb{R}$ *is a positive constant, and* $\mathbf{K}_p, \mathbf{K}_v \in \mathbb{R}^{3\times3}$ *are positive definite gain matrices. The estimate of* m *is given by* $\bar{m}$, *with the estimation error defined as* $\tilde{m} := m - \bar{m}$. *The virtual control input* $\mathbf{v}_r \in \mathbb{R}^3$ *in* (18) *is derived from the backstepping formulation. Then, the zero equilibrium of translational tracking errors* $(\tilde{\mathbf{r}}, \tilde{\mathbf{v}}) = (\mathbf{0}, \mathbf{0})$ *is globally asymptotically stable, and furthermore the mass estimation error* $\tilde{m}$ *is uniformly bounded.*

---

[1] Note that there is a slight abuse of notation here, since ϕ denotes the angle of rotation in view of axis-angle representation and has nothing to do with the roll angle previously defined for quadrotor attitude.

[2] For instance, in agricultural applications, the weight of a quadrotor with a sprayer decreases as liquid is dispersed, while for quadrotors with suspended loads, the inertia varies with changes in load position.

Proof. To show that Theorem 1 holds, we start with designing the certainty-equivalent controller by assuming perfect knowledge on m. Subsequently, we relax this assumption, accounting for the unknown mass, resulting in the final control law with adaptation. Defining the position tracking error as

$$\tilde{\mathbf{p}} := \mathbf{p} - \mathbf{p}_{\text{ref}}, \tag{19}$$

it is straightforward to design a virtual control input (18) such that if $\mathbf{v}$ perfectly tracks $\mathbf{v}_r$. Hence, the following two Lyapunov conditions are met:

$$V_1(\tilde{\mathbf{p}}) = \frac{1}{2}\tilde{\mathbf{p}}^\top \tilde{\mathbf{p}} > 0,$$

$$\dot{V}_1(\tilde{\mathbf{p}}) = \tilde{\mathbf{p}}^\top \dot{\tilde{\mathbf{p}}} = \tilde{\mathbf{p}}^\top(\mathbf{v} - \dot{\mathbf{p}}_{\text{ref}}) < 0.$$

Next, define the velocity tracking error as

$$\tilde{\mathbf{v}} := \mathbf{v} - \mathbf{v}_r, \tag{20}$$

and construct the composite Lyapunov candidate function

$$V_2(\tilde{\mathbf{p}}, \tilde{\mathbf{v}}) = V_1(\tilde{\mathbf{p}}) + \frac{1}{2}\tilde{\mathbf{v}}^\top \tilde{\mathbf{v}} > 0.$$

We can easily derive the desired (nominal) thrust vector

$$\mathbf{f} = m(-\mathbf{K}_v\tilde{\mathbf{v}} - \tilde{\mathbf{p}} - g\mathbf{e}_3 + \dot{\mathbf{v}}_r) \tag{21}$$

using backstepping technique [39] along with translation dynamics (2), such that

$$\dot{V}_2(\tilde{\mathbf{p}}, \tilde{\mathbf{v}}) = \tilde{\mathbf{p}}^\top \dot{\tilde{\mathbf{p}}} + \tilde{\mathbf{v}}^\top \dot{\tilde{\mathbf{v}}}$$

$$= \tilde{\mathbf{p}}^\top(\tilde{\mathbf{v}} - \mathbf{K}_p\tilde{\mathbf{p}}) + \tilde{\mathbf{v}}^\top(g\mathbf{e}_3 - \frac{1}{m}f\mathbf{R}\mathbf{e}_3 - \dot{\mathbf{v}}_r)$$

$$= -\tilde{\mathbf{p}}^\top\mathbf{K}_p\tilde{\mathbf{p}} + \tilde{\mathbf{v}}^\top(\tilde{\mathbf{p}} + g\mathbf{e}_3 - \frac{1}{m}f\mathbf{R}\mathbf{e}_3 - \dot{\mathbf{v}}_r)$$

$$= -\tilde{\mathbf{p}}^\top\mathbf{K}_p\tilde{\mathbf{p}} - \tilde{\mathbf{v}}^\top\mathbf{K}_v\tilde{\mathbf{v}} < 0.$$

That being said, under nominal conditions (i.e., m is perfectly known), if we choose the desired thrust and the desired body z-axis, which shall be opposite to the thrust direction, as

$$f = \|\mathbf{f}\|, \tag{22}$$

$$\mathbf{z}_{B,\text{des}} = -\frac{\mathbf{f}}{\|\mathbf{f}\|} \in \mathbb{S}^2, \tag{23}$$

then, $\tilde{\mathbf{p}}, \tilde{\mathbf{v}}$ will globally asymptotically go to zero for $t \to \infty$.

Now, we assume m to be unknown and rewrite the certainty equivalent control law (21) by replacing m with its estimate $\bar{m}$, yielding (16). To derive the adaptive law for $\bar{m}$, we construct a composite Lyapunov candidate function and take the time derivative as

$$V_3(\tilde{\mathbf{p}}, \tilde{\mathbf{v}}, \tilde{m}) = V_2(\tilde{\mathbf{p}}, \tilde{\mathbf{v}}) + \frac{1}{2\gamma_m m}\tilde{m}^2 > 0.$$

Hence,

$$\dot{V}_3(\tilde{\mathbf{p}}, \tilde{\mathbf{v}}, \tilde{m}) = \tilde{\mathbf{p}}^\top \dot{\tilde{\mathbf{p}}} + \tilde{\mathbf{v}}^\top \dot{\tilde{\mathbf{v}}} + \frac{1}{\gamma_m m}\tilde{m}\dot{\tilde{m}}$$

$$\overset{(16)}{=} -\tilde{\mathbf{p}}^\top\mathbf{K}_p\tilde{\mathbf{p}} + \tilde{\mathbf{v}}^\top\Big(\tilde{\mathbf{p}} + g\mathbf{e}_3 + \frac{\bar{m}}{m}(-\mathbf{K}_v\tilde{\mathbf{v}} - \tilde{\mathbf{p}} - g\mathbf{e}_3 + \dot{\mathbf{v}}_r)$$

$$-\dot{\mathbf{v}}_r\Big) + \frac{1}{\gamma_m m}\tilde{m}\dot{\tilde{m}}. \tag{24}$$

Recalling Assumption 3, the following equalities hold:

$$\frac{\bar{m}}{m} = 1 - \frac{\tilde{m}}{m},$$

$$\dot{\tilde{m}} = -\dot{\bar{m}},$$

which allow us to further organize (24) as

$$\dot{V}_3(\tilde{\mathbf{p}}, \tilde{\mathbf{v}}, \tilde{m}) = -\tilde{\mathbf{p}}^\top\mathbf{K}_p\tilde{\mathbf{p}} - \tilde{\mathbf{v}}^\top\mathbf{K}_v\tilde{\mathbf{v}} + \frac{\tilde{m}}{\gamma_m m}\Big(-\dot{\bar{m}}$$

$$+ \gamma_m\tilde{\mathbf{v}}^\top(\mathbf{K}_v\tilde{\mathbf{v}} + \tilde{\mathbf{p}} + g\mathbf{e}_3 - \dot{\mathbf{v}}_r)\Big). \tag{25}$$

By selecting the adaptive law for mass estimation as in (17), it can be proved that $\dot{V}_3(\tilde{\mathbf{p}}, \tilde{\mathbf{v}}, \tilde{m}) \leq 0$, which implies $\tilde{\mathbf{p}}, \tilde{\mathbf{v}}, \tilde{m} \in \mathcal{L}_\infty$, but with no guarantees on asymptotic stability. Nonetheless, we have $\dot{\tilde{\mathbf{p}}} = \tilde{\mathbf{v}} - \mathbf{K}_p\tilde{\mathbf{p}} \in \mathcal{L}_\infty$, $\bar{m} \in \mathcal{L}_\infty$ from Assumption 3, and $\dot{\mathbf{v}}_r \in \mathcal{L}_\infty$ from (18) together with

Assumption 2. Hence, it can be proved that $\dot{\tilde{\mathbf{v}}} = g\mathbf{e}_3 + \frac{1}{m}\bar{m}(-\mathbf{K}_v\tilde{\mathbf{v}} - \tilde{\mathbf{p}} - g\mathbf{e}_3 + \dot{\mathbf{v}}_r) \in \mathcal{L}_\infty$. From (20), we get $\dot{\tilde{\mathbf{v}}} = \dot{\mathbf{v}} - \dot{\mathbf{p}}_{\text{ref}} + \mathbf{K}_p\dot{\tilde{\mathbf{p}}} \in \mathcal{L}_\infty$. Therefore, $\ddot{V}_3 = -2\tilde{\mathbf{p}}^\top\mathbf{K}_p\dot{\tilde{\mathbf{p}}} - 2\tilde{\mathbf{v}}^\top\mathbf{K}_v\dot{\tilde{\mathbf{v}}} \in \mathcal{L}_\infty$, implying that $\dot{V}_3$ is uniformly continuous. By invoking Barbalat's Lemma, it can be concluded that $\lim_{t\to\infty}\dot{V}_3(t) = 0$, i.e., $\tilde{\mathbf{p}}, \tilde{\mathbf{v}} \to 0$ for $t \to \infty$. $\square$

Proposition 1 (*Robustification of Adaptive Law Using Projection Operator*). *To improve the robustness of estimation algorithms (such that parameter drift can be avoided when sensor noise exists in the system), the adaptive law of mass estimation (17) is adjusted as*

$$\dot{\bar{m}} = \text{Proj}_{\gamma_m}(\bar{m}, \tilde{v}^\top(\tilde{\mathbf{p}} + g\mathbf{e}_3 - \dot{\mathbf{v}}_r + \mathbf{K}_v\tilde{\mathbf{v}}), h),$$

where $\text{Proj}_{(\cdot)}$ *denotes* Γ-*projection [29], and the continuously differentiable convex function* $h : \mathbb{R} \times \mathbb{R} \times \mathbb{R} \to \mathbb{R}$ *is chosen as*

$$h(\bar{m}, m_0, \epsilon_m) = \frac{\bar{m}^2 - m_0^2}{2\epsilon_m m_0 + \epsilon_m^2},$$

where m_0 *and* ϵ_m *are two constant scalar quantities. If* $\bar{m}(t=0) \in \Omega_m = \{\bar{m} \in \mathbb{R} : h(\bar{m}, m_0, \epsilon_m) \leq 1\}$, *then we can conclude* $\bar{m}(t) \in \Omega_m$, *or equivalently* $\|\bar{m}(t)\| \leq m_0 + \epsilon_m, \forall t \geq 0$, *guaranteeing the boundedness of the estimated parameter.*

Proof. The readers interested in the proof of the projection operator are kindly referred to [29,40] for details. $\square$

5. Torque determination for attitude tracking

In this section, we first introduce the dynamics of attitude and angular velocity error based on the logarithmic map of SO(3). Then, we present the main results on achieving almost globally asymptotically stable tracking of attitude reference in the presence of uncertain inertia matrix through geometric control synthesis. Lastly, in the same vein as in Section 4, we also ensure the boundedness of estimation parameters by projection operator even when nonparametric uncertainties exist.

The desired orientation for attitude control can be expressed in terms of rotation matrix, which can be derived by using the heading angle reference and the desired body z-axis (23) from backstepping controller as

$$\mathbf{y}_c = [-\sin(\psi_{\text{ref}}), \cos(\psi_{\text{ref}}), 0]^\top,$$

$$\mathbf{x}_{B,\text{des}} = \mathbf{y}_c^\wedge\mathbf{z}_{B,\text{des}} / \|\mathbf{y}_c^\wedge\mathbf{z}_{B,\text{des}}\|,$$

$$\mathbf{y}_{B,\text{des}} = \mathbf{z}_{B,\text{des}}^\wedge\mathbf{x}_{B,\text{des}},$$

$$\mathbf{R}_d^i = [\mathbf{x}_{B,\text{des}}, \mathbf{y}_{B,\text{des}}, \mathbf{z}_{B,\text{des}}],$$

where $\mathbf{R}_d^i$ represents the rotation matrix from desired frame $\{\mathcal{D}\}$ to inertia frame $\{\mathcal{I}\}$. This formulation is similar to that in [38], with a slight difference due to the rotation convention used (here we use "3-2-1", while in [38] they use "3-1-2"). To address the singularity issue when $\mathbf{y}_c^\wedge\mathbf{z}_{B,\text{des}} = \mathbf{0}$ or when $\mathbf{y}_c$ and $\mathbf{z}_{B,\text{des}}$ become parallel, which can cause significant variations in the rotation matrix for minor changes in the flat output, we adopt the practical solution from [38]. This approach involves flipping signs and selecting the solution that aligns closest to the quadrotor's actual orientation, ensuring consistent desired rotation even near singularities. Since $\mathbf{R}_d^i \in SO(3)$, we can write

$$\dot{\mathbf{R}}_d^i = \mathbf{R}_d^i \, {}^{D}\boldsymbol{\omega}_{d/i}^\wedge,$$

where subscripts describe the relation of the rotational motion, e.g., $\boldsymbol{\omega}_{d/i}$ indicates the rotational motion of $\{\mathcal{D}\}$ with respect to $\{\mathcal{I}\}$.

Next, we introduce the definition of attitude and angular velocity error vector based on the logarithmic map of SO(3).

Definition 1 (*Attitude and Angular Velocity Error Vector*). For a given tracking command $(\mathbf{R}_d^i, {}^{D}\boldsymbol{\omega}_{d/i})$, and current attitude and angular velocity $(\mathbf{R}_b^i, {}^{B}\boldsymbol{\omega}_{b/i})$, we define an attitude error vector $\tilde{\mathbf{r}} : SO(3) \times SO(3) \to \mathbb{R}^3$ and an angular velocity error vector $\tilde{\boldsymbol{\omega}} : SO(3) \times \mathbb{R}^3 \times SO(3) \times \mathbb{R}^3 \to \mathbb{R}^3$

as

$$\tilde{\mathbf{r}}(\mathbf{R}_b^i, \mathbf{R}_d^i) := \log\left((\mathbf{R}_b^i)^\top \mathbf{R}_d^i\right)^\vee = \log\left(\mathbf{R}_d^b\right)^\vee, \tag{26}$$

$$\tilde{\boldsymbol{\omega}}(\mathbf{R}_b^i, {}^{\mathcal{B}}\boldsymbol{\omega}_{b/i}, \mathbf{R}_d^i, {}^{\mathcal{D}}\boldsymbol{\omega}_{d/i}) := {}^{\mathcal{B}}\boldsymbol{\omega}_{d/b} = \mathbf{R}_d^b {}^{\mathcal{D}}\boldsymbol{\omega}_{d/i} - {}^{\mathcal{B}}\boldsymbol{\omega}_{b/i}. \tag{27}$$

By Definition 1, we can derive the error dynamics of attitude and angular velocity as stated in Proposition 2. Since we are going to formulate our main results in the body frame, the $\boldsymbol{\omega}$'s in the sequel are by default expressed in $\{\mathcal{B}\}$, hence left superscripts are omitted unless ambiguities must be resolved.

Proposition 2 (*Attitude and Angular Velocity Error Dynamics*). *The dynamics of $\tilde{\mathbf{r}}$ and $\tilde{\boldsymbol{\omega}}$ satisfy*

$$\dot{\tilde{\mathbf{r}}} = \mathbf{J}_l(\tilde{\mathbf{r}})^{-1}\tilde{\boldsymbol{\omega}}, \tag{28}$$

$$\mathbf{J}\dot{\tilde{\boldsymbol{\omega}}} = \mathbf{J}\dot{\boldsymbol{\omega}}_{d/i} - \mathbf{J}\boldsymbol{\omega}_{b/i}^\wedge \boldsymbol{\omega}_{d/i} + \boldsymbol{\omega}_{b/i}^\wedge \mathbf{J}\boldsymbol{\omega}_{b/i} - \boldsymbol{\tau}, \tag{29}$$

where $\mathbf{J}_l(\cdot)^{-1}$ is the inverse of the left Jacobian as in (15).

Proof. The attitude error dynamics can be derived from (9) by using the time derivative of matrix exponential

$$\dot{\mathbf{R}}_d^b = \frac{d}{dt}\exp(\tilde{\mathbf{r}}^\wedge) = \int_0^1 \exp(\alpha\tilde{\mathbf{r}}^\wedge)\dot{\tilde{\mathbf{r}}}^\wedge \exp((1-\alpha)\tilde{\mathbf{r}}^\wedge)d\alpha$$
$$= \left(\int_0^1 (\mathbf{R}_d^b)^\alpha \dot{\tilde{\mathbf{r}}}^\wedge (\mathbf{R}_d^b)^{-\alpha}d\alpha\right)\mathbf{R}_d^b.$$

Using the definition of left Jacobian of SO(3) as given in (13) and the fact that $(\mathbf{R}\boldsymbol{\phi})^\wedge = \mathbf{R}\boldsymbol{\phi}^\wedge \mathbf{R}^\top$ [24], we can rearrange the above equation as

$$\dot{\mathbf{R}}_d^b(\mathbf{R}_d^b)^\top = \int_0^1 \left((\mathbf{R}_d^b)^\alpha \dot{\tilde{\mathbf{r}}}\right)^\wedge = \left(\mathbf{J}_l(\tilde{\mathbf{r}})\dot{\tilde{\mathbf{r}}}\right)^\wedge. \tag{30}$$

Meanwhile, we have

$$\dot{\mathbf{R}}_d^b = \mathbf{R}_d^b {}^{\mathcal{D}}\boldsymbol{\omega}_{d/b}^\wedge = \mathbf{R}_d^b(\mathbf{R}_b^d {}^{\mathcal{B}}\boldsymbol{\omega}_{d/b})^\wedge$$
$$= \mathbf{R}_d^b\left(\mathbf{R}_b^d {}^{\mathcal{B}}\boldsymbol{\omega}_{d/b}^\wedge (\mathbf{R}_b^d)^\top\right) = {}^{\mathcal{B}}\boldsymbol{\omega}_{d/b}^\wedge (\mathbf{R}_b^d)^\top = \tilde{\boldsymbol{\omega}}^\wedge \mathbf{R}_d^b. \tag{31}$$

Combining (30) and (31) yields the attitude error dynamics (28).

The angular velocity error dynamics can be derived by taking the time derivative of (27) as

$$\dot{\tilde{\boldsymbol{\omega}}} = \frac{d}{dt}(\mathbf{R}_d^b {}^{\mathcal{D}}\boldsymbol{\omega}_{d/i}) - {}^{\mathcal{B}}\dot{\boldsymbol{\omega}}_{b/i}$$
$$= \dot{\mathbf{R}}_d^b {}^{\mathcal{D}}\boldsymbol{\omega}_{d/i} + \mathbf{R}_d^b {}^{\mathcal{D}}\dot{\boldsymbol{\omega}}_{d/i} - {}^{\mathcal{B}}\dot{\boldsymbol{\omega}}_{b/i}$$
$$\overset{(27),(31)}{=} (\mathbf{R}_d^b {}^{\mathcal{D}}\boldsymbol{\omega}_{d/i} - {}^{\mathcal{B}}\boldsymbol{\omega}_{b/i})^\wedge \mathbf{R}_d^b {}^{\mathcal{D}}\boldsymbol{\omega}_{d/i} + \mathbf{R}_d^b {}^{\mathcal{D}}\dot{\boldsymbol{\omega}}_{d/i} - {}^{\mathcal{B}}\dot{\boldsymbol{\omega}}_{b/i}$$
$$= -{}^{\mathcal{B}}\boldsymbol{\omega}_{b/i}^\wedge \mathbf{R}_d^b {}^{\mathcal{D}}\boldsymbol{\omega}_{d/i} + \mathbf{R}_d^b {}^{\mathcal{D}}\dot{\boldsymbol{\omega}}_{d/i} - {}^{\mathcal{B}}\dot{\boldsymbol{\omega}}_{b/i}.$$

Multiplying both sides of the equation above by $\mathbf{J}$ and substituting $\mathbf{J}^{\mathcal{B}}\dot{\boldsymbol{\omega}}_{b/i}$ with rotational dynamics (4) yields the angular velocity error dynamics (29). □

In the sequel, we present the main results of adaptive tracking control for rotational dynamics and we require the following lemma for proving asymptotic stability.

Lemma 1 (*A Special Case of Barbalat's Lemma [29]*). *Let $f : [0, \infty) \to \mathbb{R}$. If $f, \dot{f} \in \mathcal{L}_\infty$ and $f \in \mathcal{L}_p$ for some $p \in [1, \infty)$, then $f(t) \to 0$ as $t \to \infty$.*

Theorem 2 (*Adaptive Tracking Control for Rotational Dynamics*). *Consider the attitude and angular velocity error dynamics given by (28) and (29), we define the desired control input (32) and an adaptive law for inertia matrix estimation as*

$$\boldsymbol{\tau} = \bar{\mathbf{J}}\dot{\boldsymbol{\omega}}_{d/i} - \bar{\mathbf{J}}\boldsymbol{\omega}_{b/i}^\wedge \boldsymbol{\omega}_{d/i} + \boldsymbol{\omega}_{b/i}^\wedge \bar{\mathbf{J}}\boldsymbol{\omega}_{b/i} + \mathbf{J}_l(\tilde{\mathbf{r}})^{-\top}\mathbf{K}_r\tilde{\mathbf{r}} + \mathbf{K}_w\tilde{\boldsymbol{\omega}}, \tag{32}$$

$$\dot{\bar{\mathbf{J}}} = \gamma_J(\tilde{\mathbf{e}}\dot{\boldsymbol{\omega}}_{d/i}^\top - \tilde{\mathbf{e}}\boldsymbol{\omega}_{d/i}^\top \boldsymbol{\omega}_{b/i}^\wedge - \boldsymbol{\omega}_{b/i}^\wedge \tilde{\mathbf{e}}\boldsymbol{\omega}_{b/i}^\top), \tag{33}$$

where $\gamma_J \in \mathbb{R}$ is a positive constant, and $\mathbf{K}_r, \mathbf{K}_w \in \mathbb{R}^{3\times3}$ are positive definite gain matrices. The estimate of $\mathbf{J}$ is given by $\bar{\mathbf{J}}$, with the estimation error

defined as $\tilde{\mathbf{J}} := \mathbf{J} - \bar{\mathbf{J}}$. Let $\tilde{\mathbf{e}} := \tilde{\boldsymbol{\omega}} + c\tilde{\mathbf{r}} \in \mathbb{R}^3$ be a composite error, then the zero equilibrium of rotational tracking errors $(\tilde{\mathbf{r}}, \tilde{\boldsymbol{\omega}}) = (\mathbf{0}, \mathbf{0})$ is almost globally asymptotically stable, and furthermore the inertia matrix estimation error $\tilde{\mathbf{J}}$ is uniformly bounded if the control parameter $c \in \mathbb{R}$ is selected such that

$$c \in \left(0, \min\left\{\sqrt{\frac{\lambda_r\lambda_m}{\lambda_M^2}}, \frac{4\lambda_r\lambda_w\varrho_m}{4\lambda_r\lambda_M\varrho_m\varrho_M + \lambda_w^2}\right\}\right), \tag{34}$$

where $\lambda_r := \lambda_{min}(\mathbf{K}_r)$ $\lambda_w := \lambda_{min}(\mathbf{K}_w)$ $\lambda_{\overline{w}} := \lambda_{max}(\mathbf{K}_w)$, $\lambda_m := \lambda_{min}(\mathbf{J})$, $\lambda_M := \lambda_{max}(\mathbf{J})$, and ϱ_m, ϱ_M are the lower and upper bounds of $\|\mathbf{J}_l(\tilde{\mathbf{r}})^{-\top}\|_F$, respectively.

Proof. Similar to the proof of Theorem 1, we first derive the certainty-equivalent control law by assuming perfect knowledge on $\mathbf{J}$, followed by the relaxation of such assumption and the adaptive control synthesis. Let $(\tilde{\mathbf{r}}, \tilde{\boldsymbol{\omega}}) \in S \times \mathbb{R}^3$, where $S = \{\phi\mathbf{a} : |\phi| < \pi, \mathbf{a} \in \mathbb{S}^2\}$, and consider the Lyapunov candidate function

$$V_4(\tilde{\mathbf{r}}, \tilde{\boldsymbol{\omega}}) = \frac{1}{2}\tilde{\mathbf{r}}^\top\mathbf{K}_r\tilde{\mathbf{r}} + \frac{1}{2}\tilde{\boldsymbol{\omega}}^\top\mathbf{J}\tilde{\boldsymbol{\omega}}.$$

By taking the time derivative and plugging it in the attitude and angular velocity error dynamics (28) and (29), we obtain

$$\dot{V}_4(\tilde{\mathbf{r}}, \tilde{\boldsymbol{\omega}}) = \tilde{\mathbf{r}}^\top\mathbf{K}_r\dot{\tilde{\mathbf{r}}} + \tilde{\boldsymbol{\omega}}^\top\mathbf{J}\dot{\tilde{\boldsymbol{\omega}}}$$
$$= \tilde{\mathbf{r}}^\top\mathbf{K}_r\mathbf{J}_l(\tilde{\mathbf{r}})^{-1}\tilde{\boldsymbol{\omega}} + \tilde{\boldsymbol{\omega}}^\top\left(\mathbf{J}\dot{\boldsymbol{\omega}}_{d/i} - \mathbf{J}\boldsymbol{\omega}_{b/i}^\wedge \boldsymbol{\omega}_{d/i} + \boldsymbol{\omega}_{b/i}^\wedge \mathbf{J}\boldsymbol{\omega}_{b/i} - \boldsymbol{\tau}\right)$$
$$= \tilde{\boldsymbol{\omega}}^\top\left(\mathbf{J}_l(\tilde{\mathbf{r}})^{-\top}\mathbf{K}_r\tilde{\mathbf{r}} + \mathbf{J}\dot{\boldsymbol{\omega}}_{d/i} - \mathbf{J}\boldsymbol{\omega}_{b/i}^\wedge \boldsymbol{\omega}_{d/i} + \boldsymbol{\omega}_{b/i}^\wedge \mathbf{J}\boldsymbol{\omega}_{b/i} - \boldsymbol{\tau}\right).$$

Hence, $\dot{V}_4(\tilde{\mathbf{r}}, \tilde{\boldsymbol{\omega}}) = -\tilde{\boldsymbol{\omega}}^\top\mathbf{K}_w\tilde{\boldsymbol{\omega}} \leq 0$ if the desired (nominal) torque control input is designed as[3]

$$\boldsymbol{\tau} = \mathbf{J}\dot{\boldsymbol{\omega}}_{d/i} - \mathbf{J}\boldsymbol{\omega}_{b/i}^\wedge \boldsymbol{\omega}_{d/i} + \boldsymbol{\omega}_{b/i}^\wedge \mathbf{J}\boldsymbol{\omega}_{b/i} + \mathbf{J}_l(\tilde{\mathbf{r}})^{-\top}\mathbf{K}_r\tilde{\mathbf{r}} + \mathbf{K}_w\tilde{\boldsymbol{\omega}}. \tag{35}$$

Furthermore, from $\dot{V}_4(\tilde{\mathbf{r}}, \tilde{\boldsymbol{\omega}}) = 0$, we have $\tilde{\boldsymbol{\omega}} = \mathbf{0}$, which implies $\dot{\tilde{\boldsymbol{\omega}}} = \mathbf{0}$. Using (29) we can further deduce that $\mathbf{J}\dot{\boldsymbol{\omega}}_{d/i} - \mathbf{J}\boldsymbol{\omega}_{b/i}^\wedge \boldsymbol{\omega}_{d/i} + \boldsymbol{\omega}_{b/i}^\wedge \mathbf{J}\boldsymbol{\omega}_{b/i} - \boldsymbol{\tau} = \mathbf{0}$. Lastly, using the fact that $\mathbf{J}_l(\tilde{\mathbf{r}})^{-\top}\mathbf{K}_r$ is full-rank and from (35), we conclude that $\tilde{\mathbf{r}} = \mathbf{0}$, hence showing that the largest invariant set in $S \times \mathbb{R}^3$ is the origin. By LaSalle's invariance principle, we can draw conclusions on asymptotic stability.

Then, we consider $\mathbf{J}$ to be uncertain and therefore we replace it by its estimate $\bar{\mathbf{J}}$ in the certainty-equivalent controller (35), yielding (32). To derive the adaptive law for $\bar{\mathbf{J}}$, we consider a composite Lyapunov candidate function as

$$V_5(\tilde{\mathbf{r}}, \tilde{\boldsymbol{\omega}}, \tilde{\mathbf{J}}) = V_4(\tilde{\mathbf{r}}, \tilde{\boldsymbol{\omega}}) + (c\mathbf{J}\tilde{\boldsymbol{\omega}})^\top\tilde{\mathbf{r}} + \frac{1}{2\gamma_J}\|\tilde{\mathbf{J}}\|_F^2$$
$$\geq \frac{1}{2}\lambda_m\|\tilde{\boldsymbol{\omega}}\|^2 + \frac{1}{2}\lambda_r\|\tilde{\mathbf{r}}\|^2 - c\lambda_M\|\tilde{\boldsymbol{\omega}}\|\|\tilde{\mathbf{r}}\| + \frac{1}{2\gamma_J}\|\tilde{\mathbf{J}}\|_F^2$$
$$= \zeta_1^\top\mathbf{W}_1\zeta_1,$$

where

$$\zeta_1 := [\|\tilde{\mathbf{r}}\|, \|\tilde{\boldsymbol{\omega}}\|, \|\tilde{\mathbf{J}}\|_F]^\top \in \mathbb{R}^3 \quad \text{and}$$

$$\mathbf{W}_1 := \begin{bmatrix} \frac{1}{2}\lambda_r & -\frac{1}{2}c\lambda_M & 0 \\ -\frac{1}{2}c\lambda_M & \frac{1}{2}\lambda_m & 0 \\ 0 & 0 & \frac{1}{2\gamma_J} \end{bmatrix} \in \mathbb{R}^{3\times3}.$$

Therefore, ensuring $V_5(\tilde{\mathbf{r}}, \tilde{\boldsymbol{\omega}}, \tilde{\mathbf{J}}) > 0$ is equivalent to having $\mathbf{W}_1 > 0$, or more precisely by Sylvester's criterion,

$$|c| < \sqrt{\frac{\lambda_r\lambda_m}{\lambda_M^2}}. \tag{36}$$

---

[3] Accurately determining $\dot{\boldsymbol{\omega}}_{d/i}$ is challenging. In the simulation, we compute this value through numerical differentiation, specifically applying the Euler method to approximate the derivative. Moreover, a low-pass filter is applied to smooth the signal and mitigate the impact of undesired high-frequency oscillations induced by measurement noise.

Taking the time derivative of $V_5(\tilde{\mathbf{r}}, \tilde{\boldsymbol{\omega}}, \tilde{\mathbf{J}})$ and using trace properties as well as the fact that $\mathbf{x}^\top(\mathbf{y}^\wedge\mathbf{z}) = \mathbf{y}^\top(\mathbf{z}^\wedge\mathbf{x}) = \mathbf{z}^\top(\mathbf{x}^\wedge\mathbf{y})$ holds for arbitrary vectors $\mathbf{x}, \mathbf{y}, \mathbf{z}$ with same dimension, we have

$$\dot{V}_5(\tilde{\mathbf{r}}, \tilde{\boldsymbol{\omega}}, \tilde{\mathbf{J}}) = \tilde{\boldsymbol{\omega}}^\top \mathbf{J}\dot{\tilde{\boldsymbol{\omega}}} + \tilde{\mathbf{r}}^\top \mathbf{K}_r \dot{\tilde{\mathbf{r}}} + (c\mathbf{J}\dot{\tilde{\boldsymbol{\omega}}})^\top \tilde{\mathbf{r}} + (c\mathbf{J}\tilde{\boldsymbol{\omega}})^\top \dot{\tilde{\mathbf{r}}} + \frac{1}{\gamma_J}\operatorname{tr}(\tilde{\mathbf{J}}^\top \dot{\tilde{\mathbf{J}}})$$

$$\overset{(28),(29),(32)}{=} \tilde{\boldsymbol{\omega}}^\top\big(\tilde{\mathbf{J}}\dot{\boldsymbol{\omega}}_{d/i} - \tilde{\mathbf{J}}\boldsymbol{\omega}^\wedge_{b/i}\boldsymbol{\omega}_{d/i} + \boldsymbol{\omega}^\wedge_{b/i}\mathbf{J}\boldsymbol{\omega}_{b/i} - \boldsymbol{\omega}^\wedge_{b/i}\tilde{\mathbf{J}}\boldsymbol{\omega}_{b/i}$$

$$-\mathbf{J}_l(\tilde{\mathbf{r}})^{-\top}\mathbf{K}_r\tilde{\mathbf{r}} - \mathbf{K}_w\tilde{\boldsymbol{\omega}}\big) + \tilde{\mathbf{r}}^\top\mathbf{K}_r\mathbf{J}_l(\tilde{\mathbf{r}})^{-1}\tilde{\boldsymbol{\omega}}$$

$$+c\tilde{\mathbf{r}}^\top\big(\tilde{\mathbf{J}}\dot{\boldsymbol{\omega}}_{d/i} - \tilde{\mathbf{J}}\boldsymbol{\omega}^\wedge_{b/i}\boldsymbol{\omega}_{d/i} + \boldsymbol{\omega}^\wedge_{b/i}\mathbf{J}\boldsymbol{\omega}_{b/i}$$

$$-\boldsymbol{\omega}^\wedge_{b/i}\tilde{\mathbf{J}}\boldsymbol{\omega}_{b/i} - \mathbf{J}_l(\tilde{\mathbf{r}})^{-\top}\mathbf{K}_r\tilde{\mathbf{r}} - \mathbf{K}_w\tilde{\boldsymbol{\omega}}\big)$$

$$+(c\mathbf{J}\tilde{\boldsymbol{\omega}})^\top\mathbf{J}_l(\tilde{\mathbf{r}})^{-1}\tilde{\boldsymbol{\omega}} + \frac{1}{\gamma_J}\operatorname{tr}(\tilde{\mathbf{J}}^\top\dot{\tilde{\mathbf{J}}})$$

$$= (\tilde{\boldsymbol{\omega}}^\top + c\tilde{\mathbf{r}}^\top)\tilde{\mathbf{J}}\dot{\boldsymbol{\omega}}_{d/i} - (\tilde{\boldsymbol{\omega}}^\top + c\tilde{\mathbf{r}}^\top)\tilde{\mathbf{J}}\boldsymbol{\omega}^\wedge_{b/i}\boldsymbol{\omega}_{d/i}$$

$$+(\tilde{\mathbf{J}}\boldsymbol{\omega}_{b/i})^\top(\tilde{\boldsymbol{\omega}}^\wedge\boldsymbol{\omega}_{b/i} + c\tilde{\mathbf{r}}^\wedge\boldsymbol{\omega}_{b/i})$$

$$-(\tilde{\boldsymbol{\omega}}^\top + c\tilde{\mathbf{r}}^\top)\mathbf{J}_l(\tilde{\mathbf{r}})^{-\top}\mathbf{K}_r\tilde{\mathbf{r}} - (\tilde{\boldsymbol{\omega}}^\top + c\tilde{\mathbf{r}}^\top)\mathbf{K}_w\tilde{\boldsymbol{\omega}}$$

$$+\tilde{\mathbf{r}}^\top\mathbf{K}_r\mathbf{J}_l(\tilde{\mathbf{r}})^{-1}\tilde{\boldsymbol{\omega}} + (c\mathbf{J}\tilde{\boldsymbol{\omega}})^\top\mathbf{J}_l(\tilde{\mathbf{r}})^{-1}\tilde{\boldsymbol{\omega}} + \frac{1}{\gamma_J}\operatorname{tr}(\tilde{\mathbf{J}}^\top\dot{\tilde{\mathbf{J}}})$$

$$= \operatorname{tr}\left\{\tilde{\mathbf{J}}^\top\big[-\frac{1}{\gamma_J}\dot{\tilde{\mathbf{J}}} + \tilde{\boldsymbol{\omega}}\dot{\boldsymbol{\omega}}^\top_{d/i} + \tilde{\boldsymbol{\epsilon}}\boldsymbol{\omega}^\top_{d/i}\boldsymbol{\omega}^\wedge_{b/i} - \boldsymbol{\omega}^\wedge_{b/i}\tilde{\boldsymbol{\epsilon}}\boldsymbol{\omega}^\top_{b/i}\big]\right\}$$

$$+\tilde{\boldsymbol{\omega}}^\top(c\mathbf{J}\mathbf{J}_l(\tilde{\mathbf{r}})^{-1} - \mathbf{K}_w)\tilde{\boldsymbol{\omega}} - c\tilde{\mathbf{r}}^\top\mathbf{J}_l(\tilde{\mathbf{r}})^{-\top}\mathbf{K}_r\tilde{\mathbf{r}} - c\tilde{\mathbf{r}}^\top\mathbf{K}_w\tilde{\boldsymbol{\omega}}.$$

By selecting the adaptive law for inertia matrix estimation as given in (33), we can show that

$$\dot{V}_5(\tilde{\mathbf{r}}, \tilde{\boldsymbol{\omega}}, \tilde{\mathbf{J}}) = -c\tilde{\mathbf{r}}^\top\mathbf{J}_l(\tilde{\mathbf{r}})^{-\top}\mathbf{K}_r\tilde{\mathbf{r}} + \tilde{\boldsymbol{\omega}}^\top(c\mathbf{J}\mathbf{J}_l(\tilde{\mathbf{r}})^{-1} - \mathbf{K}_w)\tilde{\boldsymbol{\omega}} - c\tilde{\mathbf{r}}^\top\mathbf{K}_w\tilde{\boldsymbol{\omega}}$$

$$\leq -c\lambda_r\varrho_m\|\tilde{\mathbf{r}}\|^2 + (c\lambda_M\varrho_M - \lambda_{\underline{w}})\|\tilde{\boldsymbol{\omega}}\|^2 + c\lambda_{\overline{w}}\|\tilde{\mathbf{r}}\|\|\tilde{\boldsymbol{\omega}}\|$$

$$= -\boldsymbol{\zeta}_2^\top\mathbf{W}_2\boldsymbol{\zeta}_2,$$

where

$$\boldsymbol{\zeta}_2 := [\|\tilde{\mathbf{r}}\|, \|\tilde{\boldsymbol{\omega}}\|]^\top \in \mathbb{R}^2 \quad \text{and}$$

$$\mathbf{W}_2 := \begin{bmatrix} c\lambda_r\varrho_m & -\frac{1}{2}c\lambda_{\overline{w}} \\ -\frac{1}{2}c\lambda_{\overline{w}} & \lambda_{\underline{w}} - c\lambda_M\varrho_M \end{bmatrix} \in \mathbb{R}^{2\times 2}.$$

That being said, $\dot{V}_5(\tilde{\mathbf{r}}, \tilde{\boldsymbol{\omega}}, \tilde{\mathbf{J}})$ is bounded from above, being semi-negative definite when $\mathbf{W}_2 > 0$, or equivalently

$$0 < c < \frac{4\lambda_r\lambda_{\underline{w}}\varrho_m}{4\lambda_r\lambda_M\varrho_m\varrho_M + \lambda_{\overline{w}}^2}, \tag{37}$$

which, together with the inequality given in (36), yields the sufficient condition (34). Hence, by far, we have shown that $\lim_{t\to\infty}V_5(t) = V_{5,\infty}$ and $\tilde{\mathbf{r}}, \tilde{\boldsymbol{\omega}}, \tilde{\mathbf{J}} \in \mathcal{L}_\infty$. Furthermore, from Eqs. (28) and (29), we can deduce that $\dot{\tilde{\mathbf{r}}}, \dot{\tilde{\boldsymbol{\omega}}} \in \mathcal{L}_\infty$. Since $\tilde{\mathbf{r}}, \tilde{\boldsymbol{\omega}} \in \mathcal{L}_2$ (by having $\int_0^\infty \boldsymbol{\zeta}_2(\tau)^\top\mathbf{W}_2\boldsymbol{\zeta}_2(\tau)d\tau \leq V_5(0) - V_{5,\infty} < \infty$), it can be then concluded using Lemma 1 that $\tilde{\mathbf{r}}, \tilde{\boldsymbol{\omega}} \to 0$ for $t \to \infty$. □

Remark 4. No assumptions were made about the symmetry of the estimated inertia matrix $\tilde{\mathbf{J}}$ (i.e., $\tilde{\mathbf{J}} = \tilde{\mathbf{J}}^\top$) throughout the proof of Theorem 2. This is due to the fact that the (direct) adaptive law (33) does not guarantee convergence to the ground truth $\mathbf{J}$; it only ensures the boundedness of the estimation error. Recognizing that the symmetric property of an inertia matrix is grounded in physics, one could explore alternative forms of adaptive laws (e.g., via indirect methods) or learning rules (e.g., neural networks) to incorporate this structural information.

Moreover, the inequality condition (37) can be obtained due to the fact that $\lambda_r, \lambda_M, \varrho_m, \varrho_M$ are positive. Observing the first two conditions is straightforward: $\mathbf{K}_r > 0$ is ensured by design, as stated in Theorem 2; rigid body inertia matrices are known to be positive semidefinite, and for quadrotors, it is positive definite, i.e., $\mathbf{J} > 0$. For ϱ_m, ϱ_M, they are the lower and upper bounds for $\|\mathbf{J}_l(\tilde{\mathbf{r}})^{-\top}\|_F$, hence being functions of $\tilde{\mathbf{r}} \in \mathcal{S} = \{\phi\mathbf{a} : |\phi| < \pi, \mathbf{a} \in \mathbb{S}^2\}$. We show their positiveness in Fig. 2, through numerical analysis in MATLAB. □

Similarly to the robustification of the adaptive law of mass estimation (17), we apply Γ-projection to (33) with the slight difference of using its matrix extension as stated in the sequel.
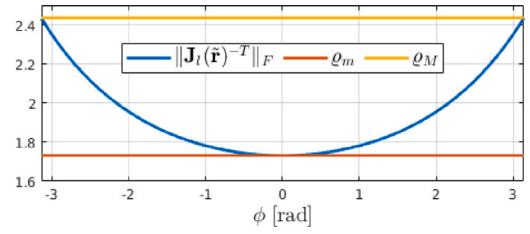

Fig. 2. Numerical analysis of the bounds of $\|\mathbf{J}_l(\tilde{\mathbf{r}})^{-\top}\|_F$ over $\mathcal{S} = \{\phi\mathbf{a} : |\phi| < \pi, \mathbf{a} \in \mathbb{S}^2\}$.

Proposition 3 (*Robustification of Adaptive Law Using Projection Operator*)**.** *The adaptive law of inertia matrix estimation (33) is adjusted as*

$$\dot{\tilde{\mathbf{J}}} = \operatorname{Proj}_{\gamma_J}(\tilde{\mathbf{J}}, \tilde{\boldsymbol{\epsilon}}\dot{\boldsymbol{\omega}}^\top_{d/i} - \tilde{\boldsymbol{\epsilon}}\boldsymbol{\omega}^\top_{d/i}\boldsymbol{\omega}^\wedge_{b/i} - \boldsymbol{\omega}^\wedge_{b/i}\tilde{\boldsymbol{\epsilon}}\boldsymbol{\omega}^\top_{b/i}, H),$$

where H consists of three continuously differentiable convex functions, specifically $H = [h_1, h_2, h_3]^\top \in \mathbb{R}^3$, with

$$h_i(\tilde{\mathbf{J}}(:, i), \mathbf{j}_0(i), \epsilon_J(i)) = \frac{\|\tilde{\mathbf{J}}(:, i)\|^2 - \mathbf{j}_0(i)^2}{2\epsilon_J(i)\mathbf{j}_0(i) + \epsilon_J(i)^2},$$

$$i = \{1, 2, 3\},$$

and $\mathbf{j}_0, \epsilon_J \in \mathbb{R}^3$ are two constant vector quantities.

6. Simulation results

In this section, we present the simulation results of our proposed controller for aggressive trajectory tracking. We start with showing the simulation environment and the corresponding settings adopted in our work, followed by presenting the tracking performance of three distinct maneuvers and the parameter estimation under uncertainties. In particular, we conduct a comparative analysis of our proposed approach against three prior studies. One of these methods utilizes the logarithmic map of SO(3) [22], while the other two rely on alternative formulations of rotational error [16,17]. Through this comparison, we demonstrate that our controller outperforms the existing approaches, particularly in effectively addressing parameter uncertainties.

6.1. Simulator

The simulation environment for evaluating our proposed controller is the Quadcopter Project[4] by MathWorks, which is based on the Parrot® series of mini-drones in MATLAB/Simulink. It consists of a nonlinear quadrotor model that includes sensors and actuators dynamics as well as dynamical environmental modeling, thereby serving as a medium-fidelity simulator for the verification of the control algorithm comparable to other simulator alternatives such as Gazebo[5] and AirSim.[6] The nominal parameters of the quadrotor are $m = 0.063$ kg, $\mathbf{J} = 1\text{e}{-4} \cdot \operatorname{diag}(0.5829, 0.7169, 1)$ kg m^2, $g = 9.8$ m/s^{-2}.

6.2. 360° flip maneuver

We first demonstrate the results of the proposed controller for performing an aggressive 360° flip maneuver. This is achieved by concatenating three control phases, as shown in Fig. 3(a). The quadrotor is commanded to first take off and stop at a hovering condition: $\mathbf{p} = (0, 0 - 4)^\top$, $\mathbf{v} = \boldsymbol{\omega} = (0, 0, 0)^\top$, $\mathbf{R} = \mathbf{I}_3$. Then, at 15 s, it is commanded to follow the desired trajectory:

$$\mathbf{R}^i_d(t) = \mathbf{I}_3 + \sin(4\pi t)\boldsymbol{\phi}^\wedge_d + (1 - \cos(4\pi t))(\boldsymbol{\phi}_d\boldsymbol{\phi}^\top_d - \mathbf{I}_3),$$

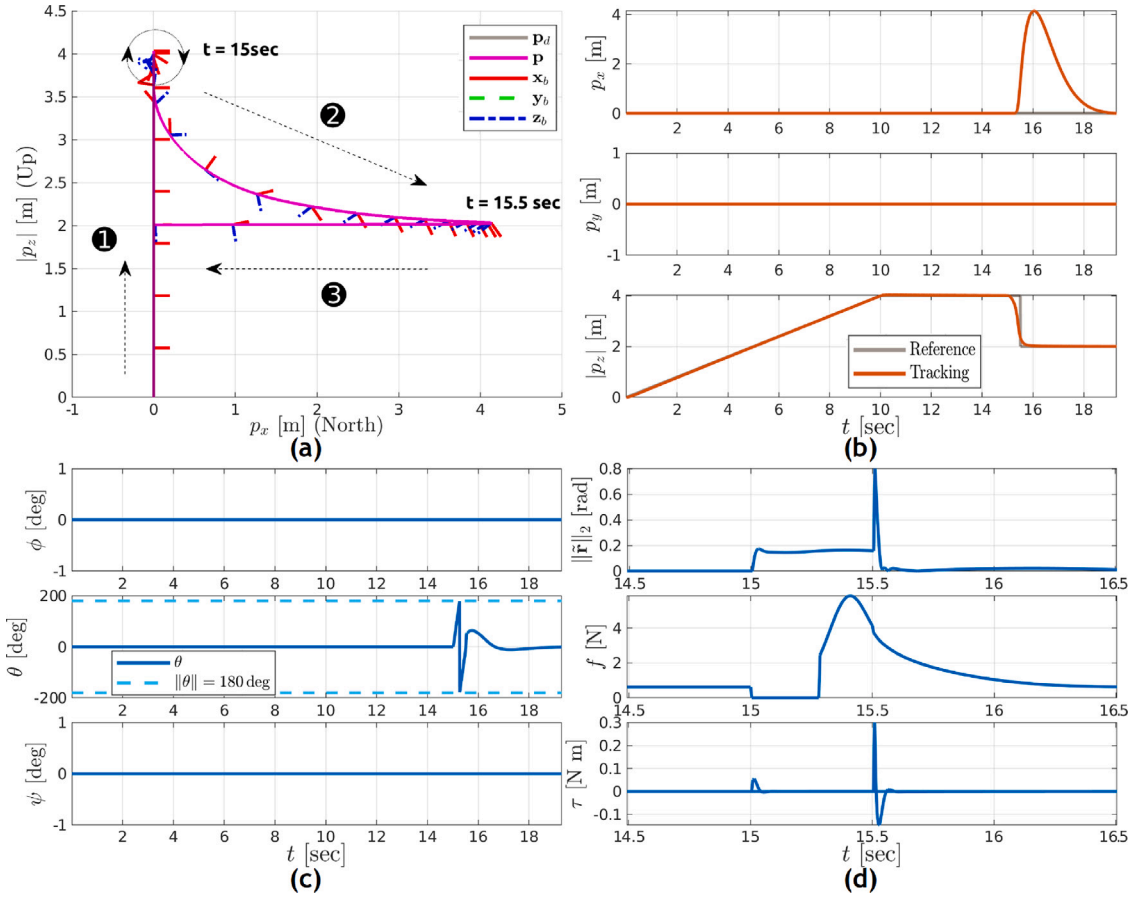**Fig. 3.** 360° **flip maneuver.** (a) Flip illustration in X-Z plane. (b) Quadrotor position **p**. (c) Euler angles ϕ, θ, ψ. (d) Attitude error $\|\tilde{\mathbf{r}}\|_2$ and control inputs $f, \boldsymbol{\tau}$.

$$\boldsymbol{\phi}_d = [0, 1, 0]^{\top},$$

which is a flipping maneuver where the quadrotor rotates about $\boldsymbol{\phi}_d$ by 360°. During the execution of such a trajectory, the backstepping controller is disabled since the control objective is to rotate the quadrotor instead of driving it to a desired position. Consequently, the desired rotation matrix is directly fed to the geometric controller as a reference signal to generate appropriate torques for attitude tracking, yielding a so-called attitude controlled flight mode [20]. Lastly, the backstepping controller is again enabled to stabilize the quadrotor at a hovering condition: $\mathbf{p} = (0, 0 - 2)^{\top}, \mathbf{R} = \mathbf{I}_3$. For this maneuver, no uncertainties are considered since the quadrotor completes the flip in under 0.1 s. Any uncertainties in the mass or inertia matrix prior to the flip will be addressed in advance.

Fig. 3(b) and (c) show the position and Euler angles, respectively, during the 360° flip. The latter illustrates the pitch angle θ that transitions from 0 to 180 deg and then from −180 deg back to 0, completing the 360° flip. Notably, during the flip around $\boldsymbol{\phi}_d$, the quadrotor deviates from its original position in x-axis, due to the temporary deactivation of the backstepping controller. The corresponding attitude error and control inputs are shown in Fig. 3(d).

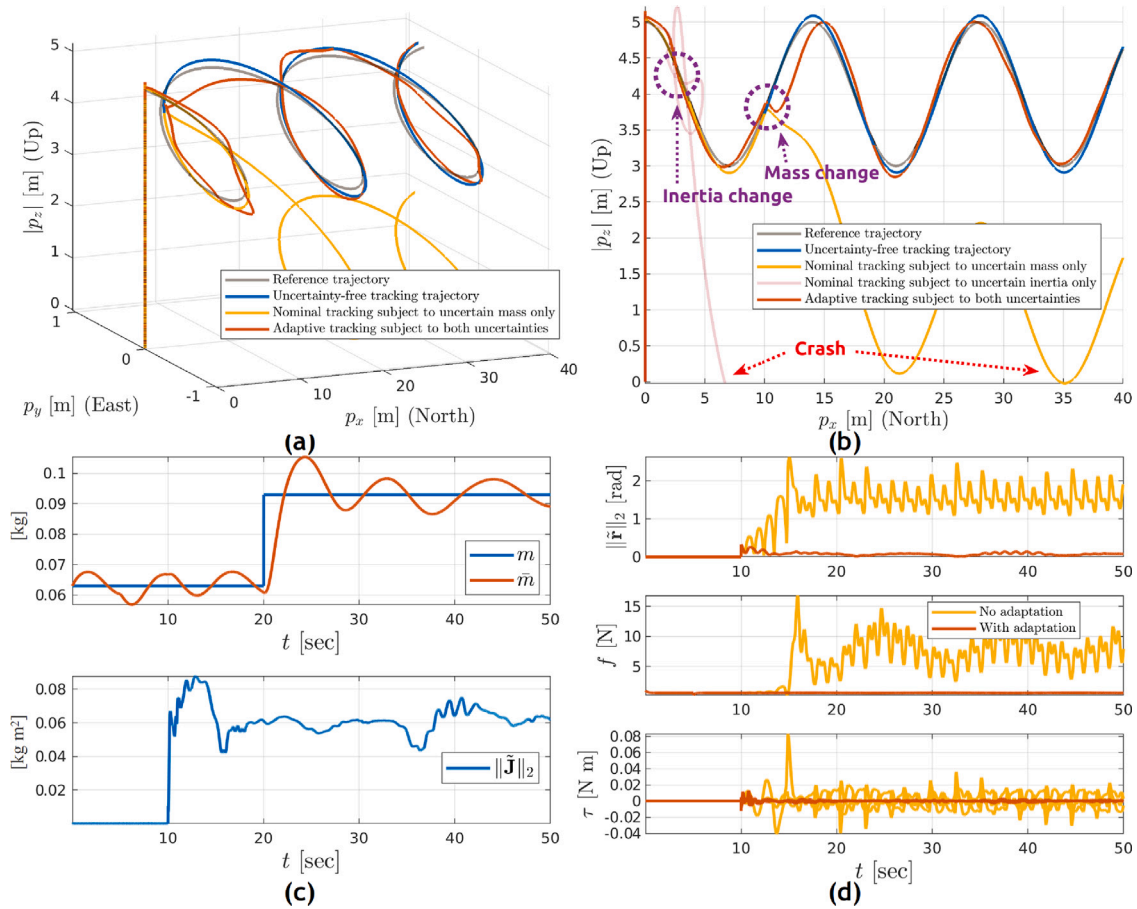### 6.3. Elliptical helix trajectory

Next, we demonstrate the ability of the quadrotor to track an elliptical helix trajectory (see Fig. 4(a)) in the presence of imprecise knowledge of the mass and inertia matrix. The quadrotor is commanded to first take off and fly to the initial position: $[\mathbf{p}^{\top}(t) \; \psi(t)] = [0, 0 - 5, 0]$, then follow the desired trajectory starting at 10 s:

$$[\mathbf{p}_{\text{ref}}^{\top}(t) \; \psi_{\text{ref}}(t)] = [t, \sin(\tfrac{\pi}{7}t), -4 - \cos(\tfrac{\pi}{7}t), \sin(0.3t)].$$

As indicated in Fig. 4(b), we introduce an increase of the inertia matrix to $\mathrm{diag}(0.0030, 0.0037, 0.0051) \; \mathrm{kg\,m}^2$ at 10 s and an increase of mass to 0.093 kg at 20 s.

To highlight the importance of our adaptive designs, we conduct a comparative analysis of the tracking performance between our proposed controller and the one in [22]. From Fig. 4(b), it can be observed that our controller successfully tracks the reference trajectory under uncertainty conditions in both mass and inertia matrix (see orange curve), whereas the controller in [22] fails for either single uncertainty (see yellow curve when only uncertain mass exists and light red curve when only uncertain inertia matrix exists), even resulting in instability. The bounded mass estimate and the estimation error of the inertia matrix are further noted for our adaptive designs in Fig. 4(c), validating Theorems 1 and 2. Moreover, the attitude error and the control inputs are presented in Fig. 4(d), from which we observe that the controller in [22] (yellow curve) is incapable of reducing the attitude error in the presence of uncertainties, thus stressing the importance as well as the effectiveness of the adaptive design in our proposed controller.

In addition, we compare our adaptive geometric controller with two prior studies that do not utilize the logarithmic map of SO(3), but instead adopt different formulations of rotational error [16,17]. As summarized in Table 1, [17] is capable of stabilizing the attitude of a rigid body with an unknown inertia matrix. Consequently, it is compared with our adaptive controller in the presence of both unknown mass and inertia matrices. In contrast, [16] only accounts for nominal conditions and fails to maintain stability when uncertainties are present. We present a numerical comparison of all four methods, including ours, in Table 2, where we report the uncertainties encountered and the Mean Square Error (MSE) of position tracking.

Fig. 4. Elliptical helix trajectory tracking. (a) 3-D visualization [†]. (b) Comparisons under nominal and uncertain scenarios. (c) Mass estimation $\bar{m}$ and inertia matrix estimation error $\|\tilde{\mathbf{J}}\|_2$. (d) Attitude error $\|\tilde{\mathbf{r}}\|_2$ and control inputs $f, \boldsymbol{\tau}$.

[†] Note that the nominal tracking subject to uncertain inertia matrix only is not shown in the 3-D visualization due to its unstable behavior, thereby resulting in a cluttered and confusing plot. For the sake of completeness, however, we put it in X-Z plane visualization in Fig. 4(b).

Table 2
Numerical comparison of elliptical helix trajectory tracking performance.

Method	Uncertainty	Position tracking MSE		
		X	Y	Z
[16]	–	0.0007	0.0019	0.0009
[17]	–	0.0008	0.0018	0.0009
Ours	–	0.0009	0.0018	0.0009
[17]	$m, \mathbf{J}$	0.0122	0.0322	0.0035
[22]	m	0.0027	0.0137	4.1671
[22]	$\mathbf{J}$	190.6881	100.2325	11.6748
Ours	$m, \mathbf{J}$	0.0043	0.0099	0.0237

The results indicate that, under nominal conditions (indicated by "-" in the uncertainty column), the performance of our controller is comparable to that of [16,17]. However, when non-parametric uncertainties are introduced, our controller outperforms the others, with [17] achieving second place. Both [16,22] suffer from instability under these conditions.

6.4. Figure-8 trajectory

Lastly, we demonstrate the effectiveness of the proposed controller in successfully executing a variety of aggressive maneuvers by tracking a high-speed Figure-8 trajectory (see Fig. 5(a)). Similar to Section 6.3, the quadrotor is first commanded to reach the starting position and then begins to track the following desired trajectory at 10 s:

$$[\mathbf{p}_{\text{ref}}^\top(t) \ \psi_{\text{ref}}(t)] = [8\cos(0.35t), 8\sin(0.7t), -4, 0].$$

In addition to the parametric uncertainties in m and $\mathbf{J}$, we also include sensor noises[7] and actuator dynamics[8] in the simulation.

From Fig. 5(b) and (d), we observe satisfactory tracking performance, particularly in horizontal coordinates, along with the corresponding motor speeds reported in RPM, respectively. The aggressive nature of the commanded maneuvers can be elucidated in Fig. 5(a) and (c), showcasing both high linear velocity with a maximum absolute value exceeding 9 m/s and large roll angles exceeding 30 deg at their maximum. It is important to emphasize that there exists potential for improvement in altitude tracking performance, which is currently compromised due to rapid alterations in both linear velocities and Euler angles. While the simulation results are omitted, it is suggested that less aggressive maneuvers can notably enhance altitude tracking performance.

7. Conclusions

In this paper, we introduced a novel adaptive geometric tracking controller tailored for quadrotor aggressive maneuvers. The control
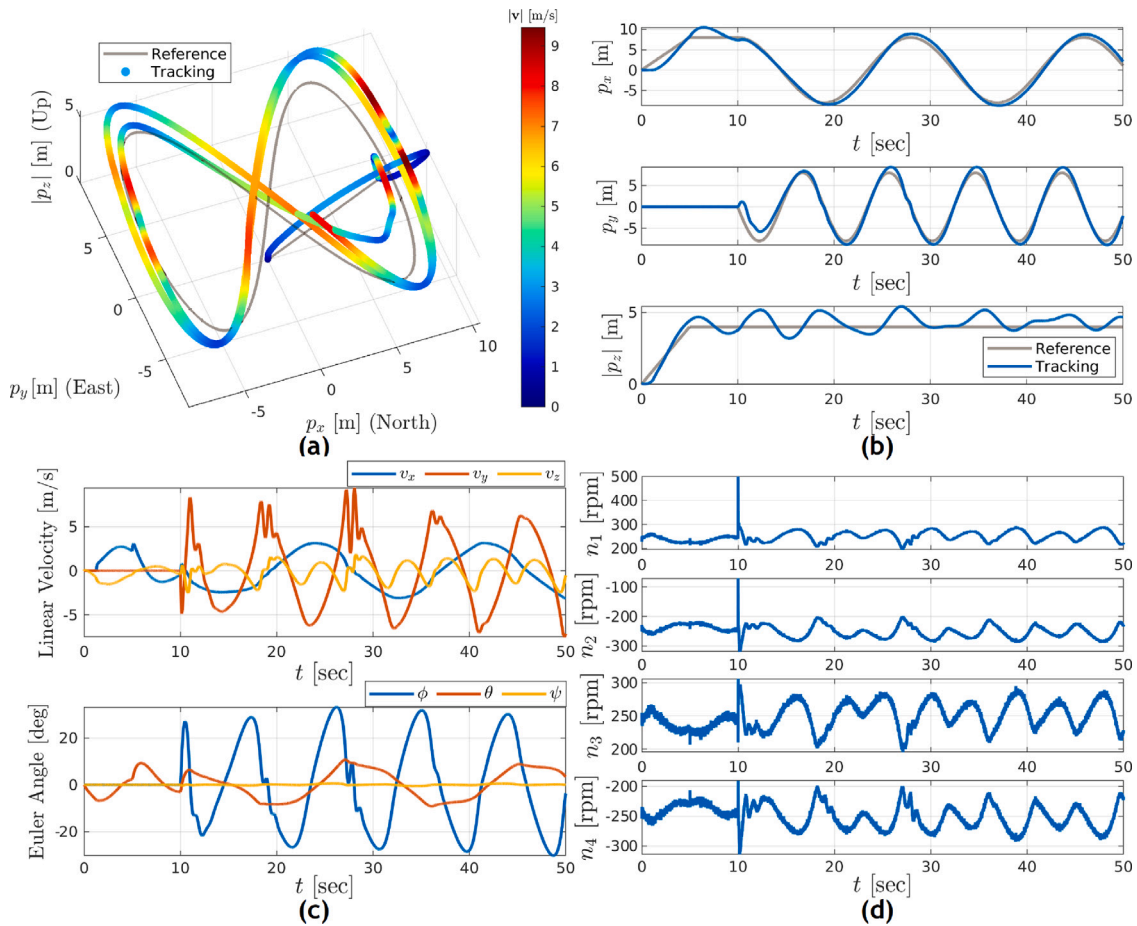
Fig. 5. Figure-8 trajectory tracking. (a) 3-D visualization with the colorbar indicating the absolute value of linear velocity. (b) Quadrotor position $\mathbf{p}$. (c) Linear velocity $\mathbf{v}$ and Euler angles ϕ, θ, ψ. (d) Motor speeds.

synthesis is inherently nonlinear, leveraging BSC for position tracking and the logarithmic map of SO(3) for attitude tracking, backed by rigorous proofs using Lyapunov analysis. The advantages of our proposed approach lie in its ability to effectively handle uncertainties, making it robust against variations in mass and inertia matrices as well as non-parametric uncertainties such as sensor noises. This is achieved through two specifically designed adaptive laws, complemented by projection operators that enhance robustness to sensor noise.

Through extensive simulations, we demonstrated the effectiveness of our proposed controller in executing various aggressive maneuvers, including a 360° flip, an elliptical helix, and a figure-8 trajectory. Notably, our controller exhibits superior performance in comparison to a recent study analogous to our approach, as well as two other methods based on alternative formulations of rotational error, thereby showcasing its applicability beyond uncertainty-free scenarios.

However, our study identified opportunities for improvement in altitude tracking during Figure-8 maneuvers, potentially influenced by rapid changes in linear velocities and Euler angles during aggressive maneuvers. Future work will focus on validating the proposed controller through real-world experimental tests, providing a practical assessment of its performance. Additionally, ongoing research aims to extend the controller to explicitly address unmodeled dynamics and disturbances, thereby broadening its applicability across a wider range of operational scenarios.

CRediT authorship contribution statement

Weibin Gu: Writing – original draft, Visualization, Validation, Methodology, Formal analysis, Data curation. **Stefano Primatesta:**

Writing – review & editing, Supervision. **Alessandro Rizzo:** Writing – review & editing, Supervision, Project administration, Funding acquisition, Conceptualization.

Declaration of competing interest

The authors declare the following financial interests/personal relationships which may be considered as potential competing interests: The authors declare that they have no known competing financial interests or personal relationships that could have appeared to influence the work reported in this paper.

Acknowledgments

Data availability

No data was used for the research described in the article.

References

[1] J. Zeng, P. Kotaru, K. Sreenath, Geometric control and differential flatness of a quadrotor UAV with load suspended from a pulley, in: 2019 American Control Conference, ACC, 2019, pp. 2420–2427, URL https://api.semanticscholar.org/CorpusID:86864412.

[2] W. Gu, D. Hu, L. Cheng, Y. Cao, A. Rizzo, K.P. Valavanis, Autonomous wind turbine inspection using a quadrotor, in: 2020 International Conference on Unmanned Aircraft Systems, ICUAS, 2020, pp. 709–715, URL https://api.semanticscholar.org/CorpusID:222221904.

[3] J.R. Goodman, J.S. Cely, T. Beckers, L.J. Colombo, Geometric control for load transportation with quadrotor UAVs by elastic cables, 2021, arXiv abs/2111.00777. URL https://api.semanticscholar.org/CorpusID:240353917.

[4] C. Huang, Z. Ming, H. Huang, Drone stations-aided beyond-battery-lifetime flight planning for parcel delivery, IEEE Trans. Autom. Sci. Eng. 20 (4) (2023) 2294–2304, http://dx.doi.org/10.1109/TASE.2022.3213254.

[5] W. Gu, K.P. Valavanis, M.J. Rutherford, A. Rizzo, UAV model-based flight control with artificial neural networks: A survey, J. Intell. Robot. Syst. 100 (2020) 1469–1491, URL https://api.semanticscholar.org/CorpusID:224852979.

[6] D. Brescianini, M. Hehn, R. D'Andrea, Quadrocopter pole acrobatics, in: 2013 IEEE/RSJ International Conference on Intelligent Robots and Systems, 2013, pp. 3472–3479, URL https://api.semanticscholar.org/CorpusID:7171094.

[7] E. Kaufmann, A. Loquercio, R. Ranftl, M. Müller, V. Koltun, D. Scaramuzza, Deep drone acrobatics, 2020, arXiv abs/2006.05768. URL https://api.semanticscholar.org/CorpusID:219559096.

[8] Y. Hou, D. Chen, S. Yang, Adaptive robust trajectory tracking controller for a quadrotor UAV with uncertain environment parameters based on backstepping sliding mode method, IEEE Trans. Autom. Sci. Eng. (2023) URL https://api.semanticscholar.org/CorpusID:264540639.

[9] X. Shao, G. Sun, W. Yao, J. Liu, L. Wu, Adaptive sliding mode control for quadrotor UAVs with input saturation, IEEE/ASME Trans. Mechatronics 27 (3) (2022) 1498–1509, http://dx.doi.org/10.1109/TMECH.2021.3094575.

[10] A.R.P. Andriën, D. Kremers, D. Kooijman, D.J. Antunes, Model predictive tracking controller for quadcopters with setpoint convergence guarantees, in: 2020 American Control Conference, ACC, 2020, pp. 3205–3210, URL https://api.semanticscholar.org/CorpusID:220891942.

[11] X. Zhang, Y. Zhuang, X. Zhang, Y. Fang, A novel asymptotic robust tracking control strategy for rotorcraft UAVs, IEEE Trans. Autom. Sci. Eng. 20 (4) (2023) 2338–2349, http://dx.doi.org/10.1109/TASE.2022.3211693.

[12] J. Stuelpnagel, On the parametrization of the three-dimensional rotation group, SIAM Rev. 6 (1964) 422–430, URL https://api.semanticscholar.org/CorpusID:13990266.

[13] S.P. Bhat, D.S. Bernstein, A topological obstruction to continuous global stabilization of rotational motion and the unwinding phenomenon, Systems Control Lett. 39 (2000) 63–70, URL https://api.semanticscholar.org/CorpusID:12699585.

[14] E.G. Hemingway, O.M. O'Reilly, Perspectives on Euler angle singularities, gimbal lock, and the orthogonality of applied forces and applied moments, Multibody Syst. Dyn. 44 (2018) 31–56, URL https://api.semanticscholar.org/CorpusID:126008906.

[15] C.G. Mayhew, R.G. Sanfelice, A.R. Teel, On quaternion-based attitude control and the unwinding phenomenon, in: Proceedings of the 2011 American Control Conference, 2011, pp. 299–304, URL https://api.semanticscholar.org/CorpusID:21303552.

[16] T. Lee, M. Leok, N.H. McClamroch, Geometric tracking control of a quadrotor UAV on SE(3), in: 49th IEEE Conference on Decision and Control, CDC, 2010, pp. 5420–5425, URL https://api.semanticscholar.org/CorpusID:6256617.

[17] T. Lee, Geometric tracking control of the attitude dynamics of a rigid body on SO(3), in: Proceedings of the 2011 American Control Conference, 2010, pp. 1200–1205, URL https://api.semanticscholar.org/CorpusID:10127449.

[18] F.A. Goodarzi, D. Lee, T. Lee, Geometric nonlinear PID control of a quadrotor UAV on SE(3), in: 2013 European Control Conference, ECC, 2013, pp. 3845–3850, URL https://api.semanticscholar.org/CorpusID:16800521.

[19] T. Lee, Robust adaptive attitude tracking on SO(3) with an application to a quadrotor UAV, IEEE Trans. Control Syst. Technol. 21 (2013) 1924–1930, URL https://api.semanticscholar.org/CorpusID:26556169.

[20] F.A. Goodarzi, D. Lee, T. Lee, Geometric adaptive tracking control of a quadrotor unmanned aerial vehicle on SE(3) for agile maneuvers, J. Dyn. Syst. Meas. Control-Trans. ASME 137 (2014) 091007, URL https://api.semanticscholar.org/CorpusID:119586168.

[21] Y. Yu, S. Yang, M. Wang, C. Li, Z. Li, High performance full attitude control of a quadrotor on SO(3), in: 2015 IEEE International Conference on Robotics and Automation, ICRA, 2015, pp. 1698–1703, URL https://api.semanticscholar.org/CorpusID:7956652.

[22] J. Johnson, R.W. Beard, Globally-attractive logarithmic geometric control of a quadrotor for aggressive trajectory tracking, IEEE Control. Syst. Lett. 6 (2021) 2216–2221, URL https://api.semanticscholar.org/CorpusID:237513916.

[23] T. Lee, Geometric control of quadrotor UAVs transporting a cable-suspended rigid body, IEEE Trans. Control Syst. Technol. 26 (1) (2018) 255–264, http://dx.doi.org/10.1109/TCST.2017.2656060.

[24] T. Barfoot, State Estimation for Robotics, Cambridge University Press, ISBN: 9781107159396, 2017, URL https://books.google.it/books?id=EpsqDwAAQBAJ.

[25] S. Teng, W. Clark, A.M. Bloch, R. Vasudevan, M. Ghaffari, Lie algebraic cost function design for control on Lie groups, in: 2022 IEEE 61st Conference on Decision and Control, CDC, 2022, pp. 1867–1874, URL https://api.semanticscholar.org/CorpusID:248266443.

[26] D. Lee, A.K. Sanyal, E.A. Butcher, Asymptotic tracking control for spacecraft formation flying with decentralized collision avoidance, J. Guid. Control Dyn. 38 (4) (2015) 587–600.

[27] D. Lee, G. Vukovich, Robust adaptive terminal sliding mode control on SE (3) for autonomous spacecraft rendezvous and docking, Nonlinear Dynam. 83 (2016) 2263–2279.

[28] F. Bullo, R.M. Murray, Proportional derivative (PD) control on the Euclidean group, 1995, URL https://api.semanticscholar.org/CorpusID:15870976.

[29] P.A. Ioannou, J. Sun, Robust adaptive control, 2012, URL https://api.semanticscholar.org/CorpusID:123201834.

[30] E. Lavretsky, K.A. Wise, Robust and adaptive control, 2013, URL https://api.semanticscholar.org/CorpusID:64058185.

[31] M. Sharma, I.N. Kar, Adaptive geometric control of quadrotors with dynamic offset between center of gravity and geometric center, Asian J. Control 23 (2020) 1923–1935, URL https://api.semanticscholar.org/CorpusID:216410045.

[32] D. Invernizzi, M. Lovera, Geometric tracking control of a quadcopter tiltrotor UAV, IFAC-Pap. 50 (2017) 11565–11570, URL https://api.semanticscholar.org/CorpusID:115273343.

[33] X.-N. Shi, Y.-A. Zhang, D. Zhou, Almost-global finite-time trajectory tracking control for quadrotors in the exponential coordinates, IEEE Trans. Aerosp. Electron. Syst. 53 (2017) 91–100, URL https://api.semanticscholar.org/CorpusID:3026071.

[34] J.S. Yeom, G. Li, G. Loianno, Geometric fault-tolerant control of quadrotors in case of rotor failures: An attitude based comparative study, 2023, arXiv abs/2306.13522. URL https://api.semanticscholar.org/CorpusID:259243941.

[35] Y. Yu, X. Ding, A global tracking controller for underactuated aerial vehicles: Design, analysis, and experimental tests on quadrotor, IEEE/ASME Trans. Mechatronics 21 (2016) 2499–2511, URL https://api.semanticscholar.org/CorpusID:489779.

[36] J. Lin, Y. Wang, Z. Miao, Q. Lin, G. Hu, R. Fierro, Robust linear-velocity-free formation tracking of multiple quadrotors with unknown disturbances, IEEE Trans. Control. Netw. Syst. 10 (4) (2023) 1757–1769.

[37] J.E. Mebius, Derivation of the Euler–Rodrigues formula for three-dimensional rotations from the general formula for four-dimensional rotations, 2007, arXiv: General Mathematics. URL https://api.semanticscholar.org/CorpusID:118133195.

[38] D. Mellinger, V.R. Kumar, Minimum snap trajectory generation and control for quadrotors, in: 2011 IEEE International Conference on Robotics and Automation, 2011, pp. 2520–2525, URL https://api.semanticscholar.org/CorpusID:18169351.

[39] P.V. Kokotovic, The joy of feedback: nonlinear and adaptive, IEEE Control. Syst. 12 (1992) 7–17, URL https://api.semanticscholar.org/CorpusID:27196262.

[40] E. Lavretsky, T.E. Gibson, Projection operator in adaptive systems, 2011, arXiv abs/1112.4232. URL https://api.semanticscholar.org/CorpusID:15452290.

[41] F. Riether, Agile quadrotor maneuvering using tensor-decomposition-based globally optimal control and onboard visual-inertial estimation, 2016, URL https://api.semanticscholar.org/CorpusID:114807752.

Weibin Gu is currently a Postdoctoral Researcher at the Institute for AI Industry Research (AIR), Tsinghua University, China. He earned his Ph.D. in Electronics and Telecommunications from Politecnico di Torino, Italy, in 2024, his M.Sc. in Mechatronic Engineering from the same institution in 2017, and his B.Sc. in Mechanical Engineering through a dual-degree program at Tongji University, China, and Politecnico di Torino in 2015. From September 2019 to October 2020, he served as a Flight Control Engineer and Project Lead at Shanghai FOIA Co., Ltd., China, where he led a UAV-based autonomous project for industrial applications. Between 2017 and 2020, he also collaborated on UAV research with the University of Denver, U.S., and Politecnico di Torino. His research interests are centered on the intersection of machine learning and control theory, with a focus on real-world robotic and autonomous systems.

Stefano Primatesta is currently an Assistant Professor in the Department of Mechanical and Aerospace Engineering. He received his Ph.D. in Computer and Control Engineering from Politecnico di Torino in 2019, his M.Sc. in Mechatronic Engineering, and his B.S in Electronic Engineering from Politecnico di Torino in 2011 and 2014, respectively. His field of research is the use of Unmanned Aircraft Systems in urban environments including virtual modeling and multi-dimensional risk analysis. His research interests include also autonomous navigation and service robotics, with applications on unmanned aerial vehicles and unmanned ground vehicles.

Alessandro Rizzo received the Laurea degree (summa cum laude) in computer engineering and the Ph.D. degree in automation and electronics engineering from the University of Catania, Italy, in 1996 and 2000, respectively. In 1998, he worked as a EURATOM Research Fellow with JET Joint Undertaking, Abingdon, U.K., researching on sensor validation and fault diagnosis for nuclear fusion experiments. In 2000 and 2001, he worked as a Research Consultant at ST Microelectronics, Catania Site, Italy, and as an Industry Professor of robotics with the University of Messina, Italy.

From 2002 to 2015, he was a tenured Assistant Professor with the Politecnico di Bari, Italy. From 2012 to 2024, he was a Visiting Professor with the New York University Tandon School of Engineering, Brooklyn, NY, USA.

In November 2015, he joined Politecnico di Torino, where he is an Associate Professor in the Department of Electronics and Telecommunications and established the Complex Systems Laboratory. Dr. Rizzo is engaged in conducting and supervising research on complex networks and systems, modeling and control of nonlinear systems, and cooperative robotics. He is the author of one book, two international patents, and about 200 papers on international journals and conference proceedings. He was a recipient of the Award for the Best Application Paper at the IFAC world triennial conference in 2002 and of the Award for the Most Read Papers in Mathematics and Computers in Simulation (Elsevier) in 2009. He has also been a Distinguished Lecturer of the IEEE Nuclear and Plasma Science Society and one of the recipients of the 2019 and 2021 Amazon Research Awards in robotics.